Eur. Phys. J. B **20**, 367–395 (2001)

THE EUROPEAN PHYSICAL JOURNAL B

EDP Sciences

Multiple domain growth and memory in the droplet model for spin-glasses

H. Yoshino[a], A. Lemaître[b], and J.-P. Bouchaud

Service de Physique de l'État Condensé, CEA Saclay, 91191 Gif-sur-Yvette Cedex, France

Received 2 November 2000

Abstract. We study domain growth dynamics when the target state is suddenly changed on all length scales. This procedure mimics the 'chaos' effect postulated by the droplet theory of spin-glasses, and allows us to investigate in details its various dynamical consequences. We study the problem by a variety of methods, including scaling arguments, analytical solution of the spherical Mattis model, and Monte Carlo simulations of a 2-dimensional Ising Mattis model. We show that successive coarsening with respect to different equilibrium states imprints multiple domain structures on top of each other, plus extra noise due to random interferences. We demonstrate that the domain structures can be retrieved by an additional series of coarsening in the reversed order which removes the noises. We discuss the rejuvenation (chaos) and memory effects observed in temperature-cycling experiments in glassy systems from the present point of view, and discuss some open problems and alternative descriptions.

PACS. 75.50.Lk Spin glasses and other random magnets – 75.10.Nr Spin-glass and other random models – 75.40.Gb Dynamic properties (dynamic susceptibility, spin waves, spin diffusion, dynamic scaling, etc.)

1 Introduction

Marginal stability of the glassy equilibrium states to weak perturbations such as a small shift of temperatures has been a fundamental interest in the studies of spin-glasses and related systems including vortex lines systems in dirty type-II super-conductors. In particular, the droplet picture based on scaling arguments and Migdal-Kadanoff type real-space renormalization-group calculations [1–4] claims that any small but finite perturbation, such as changes of temperature by an amount ΔT, is enough to change the equilibrium states in such glassy-systems completely at length scales larger than the so called overlap length $\xi_{\Delta T}$. Such a dramatic effect has been coined *temperature chaos*. It was anticipated that such a change of the equilibrium states, if it exists, should have significant consequences on dynamical observables such as the dynamical linear-susceptibility [5,6].

From the experimental side, a series of interesting experiments have been done with different spin-glasses measuring relaxations of thermo-remanent magnetization (TRM), zero-field cool magnetization (ZFC) and AC-magnetic susceptibilities. They show strikingly rich dynamical aspects of spin-glasses subjected to small temperature cycles (within the spin-glass phase) [7–16]. The main outcome of the experiments is the coexistence of two seemingly contradictory aspects, namely 'rejuvenation' upon cooling and 'memory' upon heating back. These experiments in spin-glasses have motivated similar experimental studies in other glassy systems including polymer glass [17], frozen ferrofluid [18], random ferromagnetic system [19], random ferroelectric system [20,21] and structural glass [22].

The rejuvenation effect can be interpreted as a signature of the chaotic change of the underlying equilibrium states as anticipated by the droplet picture. However the simultaneous memory effect is not obvious to account for within the droplet picture, and the previous attempts have remained unsatisfactory [5,6,13]. The need for some mechanism which allows conservation of large scale spatial structures to preserve memory is now clearly realized [14,15,23].

On the other hand, there has been recent remarkable progress in the dynamical mean-field theory for glassy systems [27–31]. It was in particular shown within the mean-field theory [31] that temperature-cycling processes

[a] *Present address:* Department of Earth and Space Science Faculty of Science, Osaka University, Machikaneyama Toyonaka 560-0043 Osaka Japan
e-mail: yoshino@.ess.sci.osaka-u.ac.jp

[b] *Present address:* Department of Physics, University of California, Santa Barbara, CA 93106 USA

amount to a cycling of break-point $q_{\rm EA}$ which separates the stationary and aging part of the correlation and response functions. The cycling of $q_{\rm EA}$ can push a part of the stationary signal into the non-stationary regime (thereby leading to rejuvenation), while preserving the rest of the non-stationary part (memory) for large enough time scales.

A somewhat similar picture was advocated within a hierarchical phase space picture [7], where each level of the hierarchical tree has its own glass temperature. Therefore, a small temperature drop drives a certain level out of equilibrium (rejuvenation) while higher level of the tree are frozen (memory) [24]. An important motivation for this picture is the Parisi's replica-symmetry breaking solution for the static properties of mean-field spin-glass models [25] This scenario has been recently substantiated by interesting numerical simulations [26]. Its real-space transcription in terms of a hierarchy of time scales associated with different length scales was developed in [23], in particular in the context of pinned domain walls [19].

In the present paper, we want to go back to the original droplet picture and work out in details the dynamical consequences of chaotic changes of the underlying equilibrium state, and in particular address the question of memory-conservation. To simplify the approach, we restrict ourselves to the simplest scenario for the relaxational dynamics as in [5]. Namely we assume that relaxational dynamics at any temperature is a coarsening process of the domain walls between an equilibrium pure state and its time-reversal state. As we noted above, changes of temperature amount to complete changes of the equilibrium states beyond $\xi_{\Delta T}$ in the droplet picture. In order to investigate the temperature cycling procedures based on the droplet picture, we have studied coarsening subjected to cycling of the underlying equilibrium state which we impose by hand. In the present paper, we disregard possible transient short-time behaviors associated with length scales smaller than $\xi_{\Delta T}$ and concentrate on the large time phenomena. Somewhat unexpectedly, we found that the domain structure corresponding to the different equilibrium states that are encountered can indeed be preserved and retrieved dynamically. We will show that the droplet picture itself can provide a suggestive and interesting scenario for the rejuvenation and memory effects observed in experiments of spin-glasses.

It is known that changes of temperature in a class of frustrated systems can change the effective coupling between certain 'block spins' due subtle entropy effects, so that interesting re-entrant phase transitions can occur [32]. This has motivated a recent work in which somewhat similar ideas for the mechanism of temperature-cycling experiments are presented [33].

The outline of the present paper is as the following. In Section 2 we briefly review the droplet picture which underlies the present study. In Section 3 we introduce our models and discuss the generic features of coarsening systems subjected to equilibrium states cycling, based on the standard phenomenology of coarsening systems. In Section 4 we study the dynamics of the $O(n)$ Mattis model in the spherical limit which is described by a time dependent Ginzburg-Landau (TDGL) equation. We solve the TDGL equation exactly under cycling of equilibrium states and examine the physical picture discussed in Section 3. In Section 5 we study 2-dimensional Ising Mattis model by Monte Carlo simulations to further check our picture. In Section 6 we compare our results with the rejuvenation (chaos) and memory effects observed in temperature-cycling experiments in a spin-glass system. Finally, in Section 7 we summarize our result and underline important open questions. In the appendices, we present some technical details of the calculations of the $O(n)$ Mattis model.

2 The droplet picture

Here we briefly review the droplet picture which is the background of the present study. For simplicity let us consider spin-glasses which have Z_2 symmetry like Ising spin-glasses. In the droplet picture, it is assumed that there exists only one equilibrium states and its time-reversal state at each temperature below the spin-glass transition temperature $T_{\rm c}$. In equilibrium, the most important contributions to physical observables such as the magnetic susceptibility comes from thermally activated excitations of compact clusters of spins, called droplets.

Let us consider for simplicity the equilibrium state at zero temperature, *i.e.* the ground state. The total number of spins at the surface of a droplet of size L is postulated to scale typically as $L_0(L/L_0)^{d_s}$ where d_s is the fractal dimension of the surface and L_0 is a microscopic length scale. By definition, a droplet of size L should have a non-zero excitation energy gap. The excitation energy of the droplet $E_{\rm gap}$ typically scales with L as $E_{\rm gap} \sim \Upsilon(L/L_0)^{\theta}$. Here Υ is the stiffness constant and θ is the stiffness exponent.

The dynamics of droplets is considered to be a thermally activated process. The energy barrier $E_{\rm barrier}$ to create a droplet is supposed to scales with L as $E_{\rm barrier} \sim \Upsilon(L/L_0)^{\psi}$ with $\psi \geq \theta$. The relaxation time is given by the Arrhenius law,

$$t_L \sim \tau_0 \exp(\Upsilon(L/L_0)^{\psi}/k_{\rm B}T), \tag{1}$$

where τ_0 is the attempt time for the activated process.

2.1 Effect of temperature change on equilibrium states

In the droplet picture, small temperature changes cause substantial changes of the equilibrium state. The argument goes as follows: the entropy associated to a droplet is the sum of contributions which are random in sign over the surface of the droplet. The latter implies the entropy associated with a droplet of size L is random in sign, and of magnitude $\sim k_{\rm B}\sqrt{(L/L_0)^{d_s}}$. A subtle conjecture is that the (free-)energy exponent θ satisfies the inequality $\theta < d_s/2$. Therefore, a small change of temperature can ruin the balance between energy and entropy. In particular, the ground state becomes unstable at finite temperatures due to the gain in entropy, and is transformed into a

'new' equilibrium state that it is completely uncorrelated with the ground state beyond the *overlap length*,

$$\frac{\xi_{\Delta T}}{L_0} \propto \left(\frac{k_{\rm B}\Delta T}{\Upsilon}\right)^{-\zeta}, \tag{2}$$

where $\zeta = 1/(d_s/2-\theta)$. It is conjectured that this kind of first-order like phase transitions occur continuously within the whole temperature range below $T_{\rm c}$.

2.2 Domain growth

Within the droplet picture[5], the aging of spin-glasses that starts from an out-of-equilibrium initial condition is thought of as a coarsening process, where the domain walls between the two equilibrium states progressively disappear. The coarsening is driven by successive nucleation and annihilation of droplets. From (1), the typical size of droplet which can be thermally activated within a given time scale t is expected to scale as,

$$L_T(t) = L_0 \left[\left(\frac{k_{\rm B}T}{\Upsilon}\log\left(\frac{t}{\tau_0}\right)\right)\right]^{1/\psi}. \tag{3}$$

Thus the mean separation of the domain walls after time t starting from a random initial condition is also expected to be given by (3).

While there is no experimental way to observe directly such a domain growth in spin-glasses, AC magnetic susceptibility can be a useful probe. In the droplet picture, the AC susceptibility at frequency ω is considered to be proportional to the inverse of the stiffness Υ of droplet excitations whose size is $L_T(\omega^{-1})$. During aging, the excitation energy gap and hence the effective stiffness is smaller than in complete equilibrium because some droplets of size $L_T(\omega^{-1})$ can happen to share their surface with the "frozen-in" droplet of size $L_T(t)$, and lower their energy. Using scaling arguments, the resultant reduction of the stiffness is obtained as $\Delta\Upsilon(L_T(\omega^{-1}), L_T(t)) \sim (L_T(\omega^{-1})/L_T(t))^{d-\theta}\Upsilon$. From the latter, the relaxation of the out-of-phase AC susceptibility is obtained as,

$$\chi''(\omega, t_{\rm w}) \sim \chi''(\omega,\infty)\left[1-\left(\frac{L_T(\omega^{-1})}{L_T(t_{\rm w})}\right)^{d-\theta}\right]^{-1}, \tag{4}$$

where $\chi''(\omega,\infty)$ is the equilibrium susceptibility. For an experimental analysis of the AC-susceptibility based on this scaling ansatz, see [76]. Some related analysis was performed also in numerical simulations of the Edward-Anderson spin-glass model [80,82]. However, the following analysis will not depend on the detailed shape of (4), but rather on the existence of some general (inverse) relation between the AC-susceptibility and the typical size of the non-equilibrium droplets.

2.3 Separation of time and length scales

An important consequence of thermally activated dynamics is that it induces a natural hierarchy of time scales (at a given temperature) and a strong separation of time scales (between different temperatures)[23]. The latter is very useful to understand the temperature cycling experiments in spin-glasses. Due to the Arrhenius law, the time needed to cross a certain energy barrier can be extremely different at two different temperatures, say T and $T+\Delta T$. The time t_T needed at temperature T to jump over a barrier crossed at time $t_{T+\Delta T}$ at temperature $T+\Delta T$ is given by:

$$t_T = \tau_0\left(\frac{t_{T+\Delta T}}{\tau_0}\right)^{1+\Delta T/T}, \tag{5}$$

or:

$$\log\left(\frac{t_T}{t_{T+\Delta T}}\right) = \frac{\Delta T}{T}\log\left(\frac{t_{T+\Delta T}}{\tau_0}\right). \tag{6}$$

The number of decades separating t_T and $t_{T+\Delta T}$ is thus equal to the number of decades separating $t_{T+\Delta T}$ and τ_0 times $\Delta T/T$. In experiments, the latter is typically 15 or so, so that a 10% temperature change multiplies the time scales by 30. Note that this separation is much weaker in numerical simulations, where the number of decades separating $t_{T+\Delta T}$ and τ_0 is ~ 5.

It is also useful to consider the separation of length scales. Let us consider two temperatures T and $T+\Delta T$. The ratio of the length scale explored at the two temperatures within the same time, say $t_{\rm w}$, is obtained from (3) as,

$$\frac{L_{T+\Delta T}(t_{\rm w})}{L_T(t_{\rm w})} = \left(1+\frac{\Delta T}{T}\right)^{-1/\psi}. \tag{7}$$

One should note that the latter formula does not imply strong separation of length scales: in order to have appreciable separation of length scale, ΔT must be comparable to T itself.

Finally it should be remarked that the time/length separation is even more sharp in reality because the typical energy barriers grow when the temperature is decreased [50]. This can be interpreted as a growth of the stiffness [5,51,81,82] as,

$$\Upsilon \sim J|1-T/T_{\rm c}|^{\psi\nu}. \tag{8}$$

3 Coarsening towards different equilibrium states

We now start to consider the possible dynamical consequences of the chaos effect within the droplet picture. Because we have in mind the temperature-cycling experiments in spin-glasses, we consider coarsening dynamics under cycling of the underlying equilibrium state. In this section we discuss intuitively how and when a succession of coarsening with respect to different states can create and store in memory the domain structures of all of them. Some essential aspects of the picture will be verified quantitatively in the following sections, based on some analytical and numerical study of the Mattis model.

To be specific, let us consider an Ising spin model on a lattice in which a spin at site i is S_i. We denote an equilibrium state as α and consider that it consists of a spin-configuration σ_i^α where σ_i^α takes ± 1 randomly with zero mean. It is convenient to introduce a projection of a spin configuration S_i to the equilibrium state σ_i^α as,

$$\tilde{S}_i^\alpha = \sigma_i^\alpha S_i. \tag{9}$$

Projections to two different ground states say $\{\sigma_i^\alpha\}$ and $\{\sigma_i^\beta\}$ are related as

$$\tilde{S}_i^\alpha = \sigma_i^\alpha \sigma_i^\beta \tilde{S}_i^\beta. \tag{10}$$

If a uniform external magnetic field $h_{\rm uni}$ is applied to the system, the Zeeman energy becomes,

$$h_{\rm uni} \sum_i S_i = \sum_i \tilde{h}_i^\alpha \tilde{S}_i^\alpha, \tag{11}$$

where we introduce a random field $\tilde{h}_i^\alpha$ defined as,

$$\tilde{h}_i^\alpha = h_{\rm uni} \sigma_i^\alpha. \tag{12}$$

In the following, we suppose that the equilibrium state at temperature T_A is a certain configuration $\alpha = \pm A$, and at temperature T_B is a different configuration $\alpha = \pm B$; we suppose that the two states A and B are completely uncorrelated beyond the overlap length $\xi_{\Delta T}$.

Concerning experiments, it should be noted that temperature is controlled within certain finite resolution δT. Thus the overlap length associated with the limited accuracy should be large enough compared with the dynamical length scales explored within some laboratory time scales. Otherwise, neither isothermal aging nor 'cycling' can even be achieved.

3.1 Mattis model

It will be useful to study a specific model which allows coarsening towards various equilibrium states in a transparent way. In later sections (Sects. 4 and 5), we analyze in detail the so called Mattis model [56],

$$H(\{S\}) = -J \sum_{i,j} \tilde{S}_i^\alpha \tilde{S}_j^\alpha - \sum_i \tilde{h}_i^\alpha \tilde{S}_i^\alpha. \tag{13}$$

As one can see easily, this model clearly has the spin-configuration $\tilde{S}_i^\alpha \equiv \pm 1$ as ground states (for $h_{\rm uni} = 0$). Since this model is equivalent to ferromagnetic models, the relaxational dynamics at low temperatures is nothing but the progressive coarsening of the equilibrium states [52]. In order to implement the droplet picture more precisely, one could introduce some disorder to the coupling parameter J in order to have thermally activated dynamics due to pinning of domain walls [57]. The latter does lead to slow growth of the domain as in (3). However, we will not perform specific analysis of the decorated model in the present paper.

In Section 4, we study coarsening of the Mattis model in the spherical limit approximation for general spatial dimension d, and obtain a fully analytical solution, which we confirm in Section 5 by a zero-temperature Monte Carlo simulation of the Mattis model in two-dimension ($d = 2$).

3.2 A cycle on a symmetry broken state

We begin with a simple cycling procedure between T_A and T_B, which provides the basic intuition about the coarsening process where the target equilibrium state is cycled. We first grow the B phase with A as the initial configuration, and then revert to A as the target state.

3.2.1 Noise imprinting

The coarsening towards B given A as the initial configuration is a standard coarsening process, because A is simply a random configuration with respect to B: the projection $\tilde{S}_i^B(t=0)$ is random in sign with short range correlation only up to $\xi_{\Delta T}$. We focus on how the symmetry-broken state A is affected by this process.

After time t, the spin-configuration $\{S_i(t)\}$ has coarsened with respect to B: the spatial pattern of the projection $\{\tilde{S}_i^B(t)\}$ consists of domains of B and $-B$ separated by domain walls. The typical distance between the domain walls is $L_{T_B}(t)$, and increases with time t. (The growth law $L_T(t)$ depend on temperature T in spin-glasses (see (3)).) The correlation between the configuration at time $t \gg \tau_0$ and the initial configuration is given by:

$$C(t,0) = (1/N) \sum_i S_i(t) S_i(0) \sim (L_T(t)/\xi_{\Delta T})^{-\lambda}. \tag{14}$$

The last equality is a general property of coarsening systems, and defines the non-equilibrium dynamical exponent λ [52]. Note that we have included the effect of short-range spatial correlations given by $\xi_{\Delta T}$ in the initial condition.

Now let us consider the projection of the spin-configuration $\{S_i(t)\}$ onto the initial state A. We expect that the projection $\{\tilde{S}_i^A(t)\}$ are random numbers with only short-ranged spatial correlation. The mean value, however, is nothing but the staggered magnetization ρ_A with respect to A which is non-zero. Indeed:

$$\begin{aligned} \rho_A(t) &\equiv (1/N) \sum_i \tilde{S}_i^A(t=0) \tilde{S}_i^A(t) \\ &= C(t,0) \sim (L_{T_B}(t)/\xi_{\Delta T})^{-\lambda}, \end{aligned} \tag{15}$$

where we have used the initial condition $\{\tilde{S}_i^A(0) \equiv 1\}$, and the simple identity $S_i(t)S_i(0) = \tilde{S}_i^A(t)\tilde{S}_i^A(0)$.

To summarize, if one starts from a completely symmetry broken state A, the coarsening with respect to a different state B adds some noise to A, and reduces the magnetization to $\rho_A(t)$ which decreases with t. However it is very important to note that *for any finite time t the bias is non-zero*: the symmetry between A and $-A$ remains broken.

3.2.2 Noise cleaning

We now revert back to A as the target state, and evolve the configuration $\{S_i(t)\}$ obtained above. The initial configuration is a random configuration with small bias $\rho = \rho_A(t)$

given in (15). Obviously the symmetry-broken state A should be finally restored, because the bias is present. An important question is the time is needed for the recovery.

If the bias ρ has been made sufficiently small, the coarsening with respect to A proceeds for a long time almost as if the initial condition was un-biased random configuration with short-range correlation of order $\xi_{\Delta T}$: both the majority (A) and minority ($-A$) phase coarsen. From the initial condition $\{S_i(t)\}$ the correlation behaves as (14) for a long time. However, in the large time limit, this correlation has to converge to ρ since the state A is finally recovered. The matching between the two regimes allows one to obtain the *recovery time* $\tau_{\rm rec}$ as:

$$\left(\frac{L_{T_A}(\tau_{\rm rec}(\rho))}{\xi_{\Delta T}}\right)^{-\lambda} \sim \rho. \tag{16}$$

This is the characteristic time around which the symmetry-broken state is *almost* recovered.

The fact that coarsening with a biased initial condition dies out after a finite time scale has been analyzed analytically in the $O(n)$ model.[53] The mechanism is similar to the interruption of coarsening under finite magnetic field studied analytically in the relaxational dynamics of the spherical Sherrington-Kirkpatrik mean field spin-glass model [54].

Now combining (15) and (16), we find a simple relation between the recovery time $\tau_{\rm rec}$ of a symmetry-broken state and coarsening time t with respect to an unrelated phase,

$$L_{T_A}(\tau_{\rm rec}) \sim L_{T_B}(t). \tag{17}$$

Note that the role of the overlap-length $\xi_{\Delta T}$ does not appear explicitly.

Here an important point in spin-glasses is that the time $\tau_{\rm rec}$ can be extremely different from t due to the strong separation of time scales (5) discussed above:

$$\tau_{\rm rec} = \tau_0 \left(\frac{t}{\tau_0}\right)^{T_B/T_A}. \tag{18}$$

In the case of negative cycling $T_A \to T_B < T_A$, the recovery time $\tau_{\rm rec}$ can be much shorter than the coarsening time t. Conversely, for positive cycling $T_A \to T_B > T_A$, the recovery time $\tau_{\rm rec}$ can be much larger than t.

3.3 Double coarsening in one step cycling

We now extend the two stage process discussed above to the following three stage process: we first coarsen the system towards A for time $t_{\rm w1}$ starting from a totally random initial configuration, unrelated to both A and B. Subsequently, we take B as the target state for a time $t_{\rm w2}$, and finally coarsen again towards A for time $t_{\rm w3}$. In spirit, this corresponds to the one-step temperature-cycling protocol used in experiments [7,8,12]. The results of the previous section corresponds to the limit where $t_{\rm w1} \to \infty$.

Fig. 1. Projection of the spin configuration onto the ground state A at end of the first stage ($t = t_{\rm w1}$). The picture is obtained by a zero-temperature Monte Carlo simulation of the 2-dimensional Ising Mattis model. The initial condition is a random initial configuration and the duration of the first stage is chosen to be $t_{\rm w1} = 1000$ MCS.

3.3.1 First and second stage

In the first stage, domains of A and $-A$ grow in competition with each other. After time $t_{\rm w1}$, the mean distance between the domain walls is $L_{T_A}(t_{\rm w1})$, that we suppose much larger than any microscopic length scale L_0 and the overlap-length $\xi_{\Delta T}$. In Figure 1 we show a picture of the domain structure of a two-dimensional Ising Mattis model (see Sect. 5) during coarsening.

Subsequently the system coarsen towards B. Since the spin configuration obtained by the first stage is a random initial configuration with respect to B, coarsening of the domains of B and $-B$ starts from the overlap length $\xi_{\Delta T}$. After time $t_{\rm w2}$, the mean separation of the domain walls is $L_{T_B}(t_{\rm w2})$ (see the upper figure of Fig. 2).

An interesting way to monitor the time evolution of the spin configuration during the second stage is to use its projection onto A (see the lower figure of Fig. 2). Remember that at the end of the first stage, the spin configuration is divided into domains of A and $-A$ separated by domain walls at a distance $L_{T_A}(t_{\rm w1})$ from each other. Let us consider such a domain as a *window cell* to monitor the time evolution of the projection onto A during the second stage. Within such a cell, the initial spin configuration is completely polarized with respect either to A or to $-A$. Then the subsequent time evolution of the spin configuration in the bulk of such a cell should be the same as the case discussed in Section 3.2.1. Thus we expect that the projection to A within the cell becomes a random configuration beyond $\xi_{\Delta T}$ but with a remnant mean bias whose sign is the same as at time $t_{\rm w1}$. The amplitude of the bias, however, decreases in magnitude as in (15).

To summarize, after time $t_{\rm w2}$ of the second stage, the projection onto A (or $-A$) is a random configuration

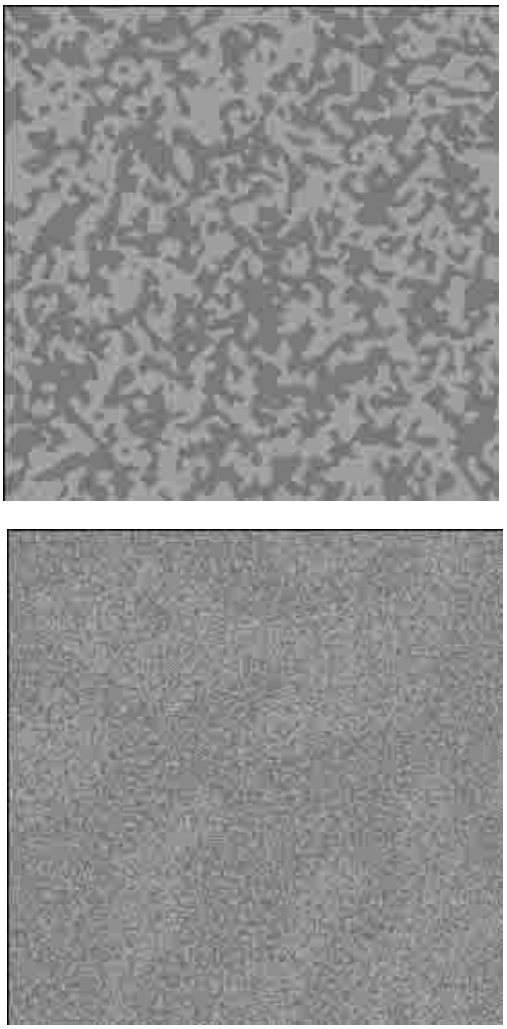

Fig. 2. The spin-configuration of the Ising Mattis model after the second stage of coarsening towards a state B, completely uncorrelated with A ($\xi_{\Delta T} = 1$). The duration is chosen to be $t_{\rm w2} = 20$ MCS, much less than $t_{\rm w1}$. The upper figure is the projection onto B whereas the lower figure is the projection onto A. One can compare the lower figure with Figure 1 and clearly distinguish the 'ghost domain' structure.

beyond $\xi_{\Delta T}$ but with a remnant local bias,

$$\rho_2 \sim (L_{T_B}(t_{\rm w2})/\xi_{\Delta T})^{-\lambda}. \tag{19}$$

The remarkable point is that the *spatial structure* of the sign of the bias, coarse-grained over the length L_{T_A} is the same as at the end of the first stage. The 'real' domain walls of size L_{T_A} which separate A and $-A$ at the end of the first stage have been destroyed. However, the 'sign' of the bias retains the very same spatial structure. For convenience, we call the latter 'ghost' domains. This is the mechanism to install and conserve memory of the thermal history of the system in the present picture.

3.3.2 Third stage

In the third stage, the state A is restored as the target state, given the final configuration of the second stage as the new initial condition. We continue to monitor the spin configuration using the window cell defined above, of size $L_{T_A}(t_{\rm w1})$. From the discussion in Section 3.2.2, coarsening of A and $-A$ re-starts within the cell. Let us call this regime the *inner-coarsening* regime.

How long does this inner-coarsening regime last? Suppose that the size of the cell $L_{T_A}(t_{\rm w1})$, which is the typical length of the spatial structure of the bias field, can be regarded as large enough so that the situation is essentially the same as with an infinitely large system with biased random initial condition (see Sect. 3.2.1). The inner-coarsening finishes at a recovery time related to the strength of the bias as given as (16). However if the size of the cell $L_{T_A}(t_{\rm w1})$ is small the inner-coarsening will be interrupted when the size of the new domains reaches that of the cell. The condition separating these two regimes reads:

$$\begin{aligned} &\text{a)}\ \ \rho_2^{-1/\lambda} \ll L_{T_A}(t_{\rm w1})/\xi_{\Delta T} \\ &\text{b)}\ \ \rho_2^{-1/\lambda} \gg L_{T_A}(t_{\rm w1})/\xi_{\Delta T} \quad (\text{'finite size effect'}). \end{aligned} \tag{20}$$

Thus we obtain the life time $\tau_{\rm rec}$ of the inner-coarsening regime as,

$$\begin{aligned} L_{T_A}(\tau_{\rm rec})/\xi_{\Delta T} &\sim \min(\rho_2^{-1/\lambda}, L_{T_A}(t_{\rm w1})/\xi_{\Delta T}) \\ \text{or} \qquad \tau_{\rm rec} &= \min\left(\tau_0 \left(\frac{t_{\rm w2}}{\tau_0}\right)^{T_B/T_A}, t_{\rm w1}\right). \end{aligned} \tag{21}$$

Let us consider the case a) more closely. In this case, a natural expectation is that after time $\tau_{\rm rec}$, the magnitude of the polarization (bias) within the bulk of the cell is almost fully recovered. The latter implies that the 'ghost' domains of sizes $L_{T_A}(t_{\rm w1})$, which are the trace of the real domain constructed in the first stage, become the 'real' domains again. The retrieved domain will then re-start to grow just as the continuation of the 1st stage. We call this regime as *outer-coarsening regime*.

An important feature is that the domain pattern retrieved after the time $\tau_{\rm rec} \ll t_{\rm w1}$ will remain almost frozen in the interval $[\tau_{\rm rec}, t_{\rm w1}]$ (see Fig. 3). Thus there is a clear separation between the inner-coarsening regime and outer-coarsening regime, when the retrieved domain structure expands appreciably. We call this intermediate regime the *plateau regime*. This is the mechanism which allows retrieval of the memory of the thermal history of the system in the present picture.

Next let us consider the case b). In this case, the noise on the 'ghost domain' is too large and the inner-coarsening finishes only at around $\tau_{\rm rec} \sim t_{\rm w1}$. The crossover from inner-coarsening to outer-coarsening takes place very smoothly and there is no plateau regime. In this case 'memory' cannot be retrieved because it is impossible to recover the amplitude of the bias with its spatial structure frozen: the shape of the domain at around $\tau_{\rm rec} \sim t_{\rm w1}$ will be already different from installed one.

To summarize, the separation of the inner-coarsening and outer-coarsening regime is different in the case a) and

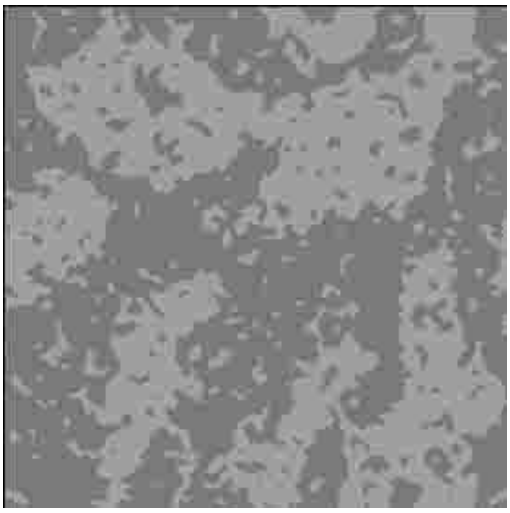

Fig. 3. The projection of the spin configuration onto the ground state A in the third stage of coarsening. The snapshot is taken after 20 MCS in the 3rd stage. Comparing with Figure 1 and Figure 2, one can find that the 'ghost domains' have become the 'real domains' again. The duration of the second stage (20 MCS) is chosen to be much smaller than that of the first stage (1000 MCS) so that the *plateau regime* exists.

b). Combining (20) and (21) we obtain,

$$\begin{aligned} &\text{a) Wide separation:} \quad L_{T_A}(\tau_{\rm rec}) \ll L_{T_A}(t_{\rm w1}) \\ &\text{b) No separation :} \quad L_{T_A}(\tau_{\rm rec}) \sim L_{T_A}(t_{\rm w1}). \end{aligned} \tag{22}$$

Remember that the amplitude ρ_2 of the bias is related to the duration of the second stage $t_{\rm w2}$ through (19). Combining the latter with the classification (22) we obtain a very simple condition:

$$\begin{aligned} &\text{a) Wide separation:} \quad L_{T_B}(t_{\rm w2}) \ll L_{T_A}(t_{\rm w1}) \\ &\text{b) No separation :} \quad L_{T_B}(t_{\rm w2}) \sim L_{T_A}(t_{\rm w1}). \end{aligned} \tag{23}$$

Thus the separation between the inner- and outer-coarsening regimes in the third regime depends on relative domain size in the first and second stages.

Finally, let us note for completeness what is happening on the projection onto B during the 3rd stage: the projection onto B is becoming more and more noisy but still the 'ghost domains' of size $L_{T_B}(t_{\rm w2})$, which is the remnant of the 'real domains' of B created in the second state, remain.

3.4 AC susceptibility in one step cycling

It is useful to consider how the double coarsening can be observed through the AC susceptibility. Within the droplet picture, the relaxation of the AC susceptibility is due to the decrease of the domain wall density (see Sect. 2.2). The specific scaling form (4) is derived for standard isothermal aging where $L(t_{\rm w})$ is the size of the domain monotonically increasing with time. In the case of the one step cycling, we only need to replace $L(t_{\rm w})$ by the relevant domain size.

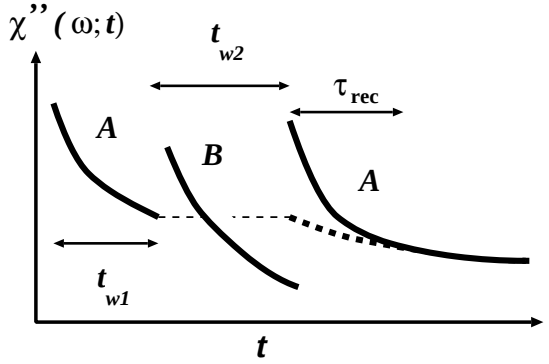

Fig. 4. Schematic behavior of the relaxation of the out-of-phase AC-susceptibility in an one-step cycling procedure. The thick dotted line is the reference curve which is the direct continuation of the first stage. 'A' and 'B' indicate which equilibrium state is coarsening.

In the first stage ($0 < t < t_{\rm w1}$) , the susceptibility simply decays as standard aging (4) where the relevant size of the domain is that of the A phase $L_{T_A}(t)$. In the second stage ($t_{\rm w1} < t < t_{\rm w1} + t_{\rm w2}$), the relevant domains are that of the B phase so the relevant length scale is now $L_{T_B}(t - t_{\rm w1})$. Thus the relaxation re-starts and there is a discontinuity at $t = t_{\rm w1}$, as clearly observed in many experiments [7,8,12].

In the previous section, we argued that the third stage ($t_{\rm w1}+t_{\rm w2} < t$) can be divided into two asymptotic regimes, namely, an inner-coarsening regime for ($t_{\rm w1} + t_{\rm w2} < t \ll t_{\rm w1} + t_{\rm w2} + \tau_{\rm rec}$) and an outer-coarsening regime for ($t_{\rm w1} + t_{\rm w2} + \tau_{\rm rec} \ll t$).

In the inner-coarsening regime, the relevant size of domain is $L_{T_A}(t - t_{\rm w1} - t_{\rm w2})$. Thus the relaxation of the AC-susceptibility re-starts and there is again a discontinuity at $t = t_{\rm w1} + t_{\rm w2}$. This feature can be observed only if the frequency ω of the AC field is large enough compared with the inverse lifetime of the inner-coarsening regime,

$$\omega^{-1} \ll \tau_{\rm rec}. \tag{24}$$

On the other hand, in the outer-coarsening regime the relevant domain is that of the revived ghost domains. Thus in the latter regime, the relevant size of the domain is simply $L_{T_A}(t - t_{\rm w2})$ and the relaxation of the AC-susceptibility is the continuation of the first stage as if the second stage were absent. This can be observed if the experiment is continued up to large enough time $t_{\rm w3}$ compared with the lifetime of the inner-coarsening regime,

$$t_{\rm w3} \gg \tau_{\rm rec}. \tag{25}$$

We summarize the generic behavior of the relaxation of the out-of-phase AC-susceptibility in the one-step cycling procedure in Figure 4. Here a very important remark is that the strong separation of time scale (5) in spin-glasses due to the activated dynamics can explain the strong differences in the third regime between negative and positive cycling observed in experiment (this point was emphasized in [13,6]). In the case of negative cycling, the outer-coarsening regime can be easily observed but the

lifetime of the inner-coarsening regime can be so short that (24) is not satisfied. On the contrary, positive cycling makes the inner-coarsening regime easily observed (rejuvenation) but its effect is rapidly too large to allow the observation of some 'memory'. As we will discuss later in Section 6, the experimental data can be (at least qualitatively) interpreted along these lines.

3.5 Relaxation of DC susceptibilities after one-step cycling

Another powerful experimental tool to study the temperature-cycling process is the DC-magnetic susceptibilities in the third stage of the one-step cycling. In a class of experiments [7], very small magnetic field h is applied during temperature-cycling $T_1(t_{\rm w1}) \to T_2(t_{\rm w2}) \to T_1(t_{\rm w3})$. The magnetic field is then cut-off at time

$$t_{\rm w}^{\rm total} \equiv t_{\rm w3} + t_{\rm w2} + t_{\rm w1} \tag{26}$$

and relaxation of the magnetization (thermo-remanent magnetization (TRM)) is measured subsequently at time $\tau + t_{\rm w}^{\rm total}$ with increasing τ in the third stage where the temperature is kept to T_1.

As far as linear-response holds, the magnetization can be written as $h\chi_{\rm TRM}(\tau + t_{\rm w}^{\rm total}, t_{\rm w}^{\rm total})$ where we introduced a dynamical DC-magnetic susceptibility. In another class of experiments[12], the temperature cycling is done under zero-field. Then a small magnetic field is switched on and the growth of the magnetization (zero-field cooled magnetization (ZFC)) is measured. Again the magnetization can be written as $h\chi_{\rm ZFC}(\tau + t_{\rm w}^{\rm total}, t_{\rm w}^{\rm total})$ where we introduced another dynamical DC-magnetic susceptibility. As far as linear response holds, the TRM and ZFC are simply related [12] as

$$\chi_{\rm ZFC}(\tau + t_{\rm w}^{\rm total}, t_{\rm w}^{\rm total}) + \chi_{\rm TRM}(\tau + t_{\rm w}^{\rm total}, t_{\rm w}^{\rm total}) = \chi_{\rm ZFC}(\tau + t_{\rm w}^{\rm total}, 0). \tag{27}$$

The rightside of the last equation is the magnetization (divided by h) measured if the magnetic field is applied from the beginning and afterwards. Experimentally such a magnetization almost saturates to a constant which is oftenly called as field cool (FC) magnetization. If one assumes *naively* that the fluctuation dissipation theorem (FDT) holds, the DC-susceptibilities (per spin) are related to auto correlation function $C(\tau + t_{\rm w}^{\rm total}, t_{\rm w}^{\rm total}) \equiv \langle m(\tau + t_{\rm w}^{\rm total}) m(t_{\rm w}^{\rm total})\rangle$ of magnetization $m(t)$ (per spin). Assuming that the correlation function is normalized as $C(t,t) = 1$ one finds the ZFC susceptibility as,

$$\chi_{\rm ZFC}(\tau + t_{\rm w}^{\rm total}, t_{\rm w}^{\rm total}) = (k_{\rm B}T)^{-1}(1 - C(\tau + t_{\rm w}^{\rm total}, t_{\rm w}^{\rm total})). \tag{28}$$

and the TRM susceptibility $\chi_{\rm TRM}(\tau + t_{\rm w}^{\rm total}, t_{\rm w}^{\rm total})$ is related *via* (27).

Let us now consider the one-step cycling protocol. Suppose that the magnetic field is applied during the 1st and 2nd stage and then cut-off right at the beginning of the third stage, *i.e.* $t_{\rm w3} = 0$ so that $t_{\rm w}^{\rm total} = t_{\rm w2} + t_{\rm w1}$. Then TRM magnetization at time $\tau + t_{\rm w}^{\rm total} = \tau + (t_{\rm w2} + t_{\rm w1})$ should relax with increasing τ just like the auto-correlation function between the magnetization right at time $t_{\rm w2} + t_{\rm w1}$ and that after time τ later. From the discussions in the previous sections, we expect that auto-correlation function will be generically the following,

$$C(\tau + (t_{\rm w2} + t_{\rm w1}), t_{\rm w2} + t_{\rm w1}) = \begin{cases} C_0(\tau, 0) & L(\tau) \ll L(\tau_{\rm rec}(\rho)) \quad \text{inner-coarsening} \quad (29) \\ \rho C_0(\tau + t_{\rm w1}, t_{\rm w1}) & L(\tau) \gg L(\tau_{\rm rec}(\rho)) \quad \text{outer-coarsening,} \quad (30) \end{cases}$$

where C_0 is the auto-correlation function in the standard coarsening (14) and ρ is the amplitude of the ghost domain right after the 2nd stage, which decreases for larger $t_{\rm w2}$. We have confirmed the above feature analytically within the spherical Mattis model (see Fig. 6) in Section 4.5 and numerically in two-dimensional Ising Mattis model (see Fig. 9) in Section 5. It is interesting to note that quite similar features have also been obtained within the dynamical mean-field theory [31] in the sense that the effect of the second stage amounts to a reduction of the plateau value $q_{\rm EA}$ at which the rejuvenation and memory effects are separated.

Here we are assuming the case a) $L(t_{\rm w1}) \gg L(t_{\rm w2})$ which allows clear separation between the inner- and outer-coarsening regimes. The initial decay is that due to the inner-coarsening regime, $(L(\tau) \ll L(\tau_{\rm rec}))$ where the correlation decays as if the memory of the first stage was completely lost. The remarkable feature is the plateau regime $L(\tau_{\rm rec}) \ll L(\tau) \ll L(t_{\rm w1})$, where the correlation function stays almost constant. The subsequent drop is due to the outer coarsening $L(t_{\rm w1}) \ll L(\tau)$ where the correlation function decays as if the second stage is absent. But here the amplitude is reduced from 1 to ρ. Note that in the limit $L(t_{\rm w1}) \to \infty$, the second relaxation does not occur $C_0(\tau + t_{\rm w1}, t_{\rm w1}) = 1$. The latter is the same as the case of a cycling on a symmetry broken state discussed in Section 3.2.2.

In the previous TRM experiments [7], the field change is made not right at the beginning of the third stage but slightly afterwards when some additional time $t_{\rm w3}$ is spent in the third stage. The auto correlation corresponding to the DC-magnetic susceptibilities is now $C(\tau + t_{\rm w}^{\rm total}, t_{\rm w}^{\rm total} (= t_{\rm w3} + t_{\rm w2} + t_{\rm w1}))$ with non-zero $t_{\rm w3} > 0$. The behavior becomes more complicated because the noise is already removed to a certain extent during the additional period $t_{\rm w3}$ thus the effect of rejuvenation tends to be obscured. Nonetheless we explicitly compute such an auto-correlation function in Section 4.5 and later compare with experimental curves in Section 6.

Finally let us note that standard FDT assumed above naively does not hold in non-stationary dynamics as the one we are concerned here. It is by now well known [27,29,30] that in spin-glass systems one should consider modified forms of FDT. As compared with the AC-susceptibility discussed in the previous section, DC-susceptibilities contain integral contributions of wider

range of the non-stationary parts of the response function where the standard FDT is very likely violated. Unfortunately, the conventional droplet picture [2,5] is not able to take into account strongly non-stationary part of responses in spin-glasses. Recent progress of the dynamical mean-field theories [27–29] suggests that it can be quite different from usual coarsening systems. Nonetheless, *qualitative* features of relaxation curves of auto-correlation functions and DC-magnetic susceptibilities, such as the waiting time effects, are known to be very similar in the case of isothermal aging. The latter implies that qualitative feature discussed above concerning the relaxation after temperature-cycling also applies for the DC-magnetic susceptibilities.

3.6 Multiple coarsening in multiple step cycling

One can naturally extend the one step cycling to multiple steps cycling of the equilibrium states which try to mimic continuous temperature-cycling experiments [12,15]. For example, let us consider the coarsening of three different equilibrium states A, B and C which take place in turn as $A \to B \to C$ with durations $t_{\rm w1}$, $t_{\rm w2}$ and $t_{\rm w3}$ respectively. Since we are interested with large time behaviors, we disregard the differences between the corresponding overlap lengths and simply set them to the microscopic length L_0. At the beginning of each stage, a new coarsening process is started. After the first, second and third stages, the domain sizes of A, B and C are $L_{T_A}(t_{\rm w1})$, $L_{T_B}(t_{\rm w2})$ and $L_{T_C}(t_{\rm w3})$ respectively.

Let us consider the noise imprinted on the projected configuration (onto the reference state) due to the coarsening of unrelated phases. The second stage reduces intensity of the bias of the A phase from 1 down to $\rho_A(t_{\rm w1}+t_{\rm w2}) \sim (L_{T_B}(t_{\rm w2})/L_0)^{-\lambda}$. Similarly, the third stage reduces the bias of the B phase down to, $\rho_B(t_{\rm w1}+t_{\rm w2}+t_{\rm w3}) \sim (L_{T_C}(t_{\rm w3})/L_0)^{-\lambda}$. An interesting question is how the third stage influences the projection onto the A phase. A natural expectation is that the noise effect is *multiplicative*[1],

$$\rho_A(t_{\rm w3}+t_{\rm w2}+t_{\rm w1}) \sim \rho_A(t_{\rm w1}+t_{\rm w2})(L_{T_C}(t_{\rm w3})/L_0)^{-\lambda} \sim (L_{T_B}(t_{\rm w2})/L_0)^{-\lambda}(L_{T_C}(t_{\rm w3})/L_0)^{-\lambda}. \quad (31)$$

To summarize, we obtain a 'real' domain of phase C with size $L_{T_C}(t_{\rm w3})$ and 'ghost' domains of phases A and B, with sizes $L_{T_A}(t_{\rm w1})$ and $L_{T_B}(t_{\rm w2})$ respectively but with reduced intensities. Thus the information of all the three phases are now stored in the spin configuration but with noises due to random interferences.

Now let us consider how we can retrieve memories installed above by removing the noise that blurred stored information. Here we have to remember that memory can be retrieved by additional conjugate coarsening but only in the case a): when the noise is small enough (see (20–23)).

[1] We explicitly verify this relation within the $O(n)$ Mattis model in Appendix B.

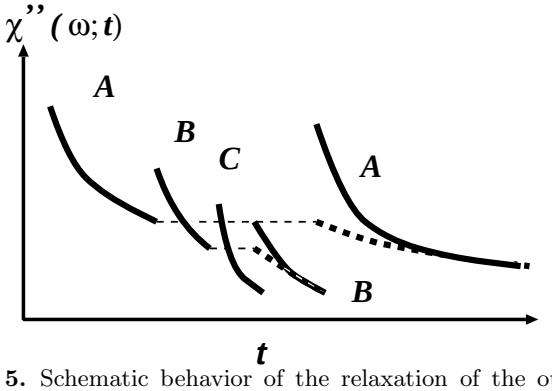

Fig. 5. Schematic behavior of the relaxation of the out-of-phase AC-susceptibility in a two-step cycling procedure. Thick dotted lines are the reference curves which show direct continuation of the second and first stages. 'A', 'B' and 'C' indicate the equilibrium states which are coarsening.

To be specific, let us suppose that the previous coarsening of A, B, and C is done in a well separated manner in the sense that $t_{\rm w1} \gg \tau_0(t_{\rm w2}/\tau_0)^{T_B/T_A}$ and $t_{\rm w2} \gg \tau_0(t_{\rm w3}/\tau_0)^{T_C/T_B}$. Then let us consider reversed order coarsening of the above procedure. First, we perform coarsening of B with durations $t'_{\rm w2}$ given the final spin configuration obtained above. According to the result of the previous section, it is sufficient to choose the duration $t'_{\rm w2} \sim \tau_{\rm rec} = \tau_0(t_{\rm w3}/\tau_0)^{T_C/T_B}$ to remove the noise on B due to C and recover the spin configuration just before the coarsening of C. We will not choose a larger $t'_{\rm w2}$ in order to avoid the outer-coarsening of B which adds some additional noise to A, which will be treated later. Second we perform coarsening of A. By the same argument, it will be again enough to choose its duration as $t'_{\rm w1} \sim \tau_{\rm rec} = \tau_0(t_{\rm w2}/\tau_0)^{T_B/T_A}$.

If one skips the 2nd coarsening of B and try to remove the noise by doing only the 2nd coarsening of A, the time need for the recovery $\tau_{\rm rec}$ will become astronomically large,

$$(L(\tau_{\rm rec})/L_0)^{-\lambda} = \rho_A\rho_B \qquad \text{or}$$
$$\tau_{\rm rec} = \tau_0(t_{\rm w2}/\tau_0)^{(T_B/T_A)(T_B/T_A)\log(t_{\rm w3}/\tau_0)} \quad (32)$$

Thus it is very important that the multiplicative noise is cured in two steps and not by a single stroke.

More generally one can perform successive coarsening of arbitrary number of phases $A_1 \to A_2 \ldots \to A_n$ with durations $t_{\rm w2}$, $t_{\rm w3}$, …, t_{wn} followed by the reversed processes $A_{n-1} \to A_{n-2} \ldots \to A_1$ with durations t'_{n-1}, t'_{n-2}, …, t'_1. The retrieval of the memory of each phase is ensured by the condition,

$$t_i \gg \tau_0(t_{i+1}/\tau_0)^{T_{i+1}/T_i} \qquad t'_i \sim t_i. \quad (33)$$

Note that this can be easily realized in a negative cycling. The domain structures of all the phases will be retrieved one after another[2]. The behavior of the AC-susceptibility during such a multi-step (continuous) cycling will be interesting. The generic behavior will be 'hierarchical' as depicted schematically in Figure 5. In Section 6, we discuss

[2] The phases of large i which are recovered earlier become noisy again as phases of smaller i are treated later.

recent continuous temperature-cycling experiments from this point of view.

4 The O(n) mattis model

In the previous section we discussed the peculiar properties of coarsening under a cycling of the equilibrium states, based on scaling and heuristic arguments. In this Section we study the Mattis model introduced in Section 3.1 in the spherical limit. This allows us to explicitly solve the dynamical equation under one-step cycling of the equilibrium states and check in details the physical picture presented in the above sections. This section is rather technical and can be skipped at first reading (the previous section is indeed the summary of the study in the present section and Sect. 5). The reader interested by a more physical discussion can go directly to Section 6.

4.1 Model and definitions

4.1.1 Dynamics of projection field

Here we generalize the projection field $\tilde{S}$ to be a n-dimensional vector field $\boldsymbol{\phi}(x,t)$ continuously varying in a d-dimensional space. The time evolution of the projection field $\boldsymbol{\phi}(x,t)$ is given by the time dependent Ginzburg-Landau (TDGL) equation,

$$\frac{\partial \boldsymbol{\phi}}{\partial t} = -\frac{\delta F_{[\boldsymbol{\phi}]}}{\delta \boldsymbol{\phi}}, \tag{34}$$

with the free-energy functional defined as,

$$F_{[\boldsymbol{\phi}]} = \int \mathrm{d}^d x \left[\frac{1}{2}(\nabla \boldsymbol{\phi})^2 + \alpha \frac{(n-|\boldsymbol{\phi}|^2)^2}{4n} \right]. \tag{35}$$

Here we disregard the Langevin force due the to thermal noise on the dynamics because the latter is irrelevant in the present model [52].

In the spherical limit $n \to \infty$, under the assumption of self-averageness, any one of the component satisfies,

$$\frac{\partial \phi}{\partial t} = \nabla^2 \phi - z(t)\phi, \tag{36}$$

with

$$z(t) = \mu(1 - \langle \phi^2(t) \rangle), \tag{37}$$

where $\langle ... \rangle$ means expectation value. Thus we only need to consider a single component, *i.e.* a scalar field in the following.

4.1.2 Random equilibrium states

We suppose that the equilibrium configuration is represented by a random scalar field $\sigma(x)$. The spin configuration $\psi(x)$ is related to the projection field as,

$$\psi(x) = \sigma(x)\phi(x), \tag{38}$$

which is equivalent to the relation (9) on the lattice. We assume that $\sigma(x)$ is a Gaussian random scalar field with zero mean,

$$\langle \sigma(x) \rangle_\sigma = 0 \tag{39}$$

and short-ranged spatial correlations,

$$\langle \sigma(x)\sigma(x') \rangle_\sigma = \Delta \delta^d(x-x'). \tag{40}$$

The latter means that we essentially disregard the finiteness of the overlap length (2). One could include this effect by introducing a short-range correlated Gaussian field. However since we are focusing on large time behavior, we do not go into such details in the present paper.

As for the lattice case (10), the projections to different equilibrium states, say α and β, are related as,

$$\phi^\alpha(x) = \sigma^{\alpha\beta}(x)\phi^\beta(x). \tag{41}$$

where we defined a 'transformation field',

$$\sigma^{\alpha\beta}(x) \equiv \sigma^\alpha(x)\sigma^\beta(x). \tag{42}$$

The transformation field should be also a random field with zero mean,

$$\langle \sigma^{\alpha\beta}(x) \rangle_\sigma = 0 \tag{43}$$

and short-ranged correlation,

$$\langle \sigma^{\alpha\beta}(x)\sigma^{\alpha\beta}(x') \rangle_\sigma = \Delta \delta^d(x-x'). \tag{44}$$

More generally we have,

$$\langle \sigma^{\alpha_1\alpha_2}(x_1)\sigma^{\alpha_2\alpha_3}(x_2)\dots\sigma^{\alpha_{n-1}\alpha_n}(x_{n-1})\sigma^{\alpha_n\alpha_1}(x_n) \rangle_\sigma = \Delta^n \delta^d(x_1-x_2)\delta^d(x_2-x_3)\dots\delta^d(x_{n-1}-x_n). \tag{45}$$

Some useful statistical properties of the transformation field are presented in Appendix A.

4.1.3 Formal solution

Taking Fourier transform $\hat{\phi}_k = \int \mathrm{d}^d x \phi(x) \mathrm{e}^{\mathrm{i}kx}$, one finds the formal solution to the TDGL equation (36) as,

$$\hat{\phi}_k(t) = \hat{\phi}_k(t') \frac{\mathrm{e}^{-k^2(t-t')}}{\sqrt{\Gamma(t,t')}}, \tag{46}$$

where we introduced

$$\Gamma(t,t') = \exp\left(2 \int_{t'}^{t} \mathrm{d}t' z(t') \right). \tag{47}$$

Note that details of the solution are absorbed in $\Gamma(t,t')$. By definition one must have the identity,

$$\Gamma(t,t) = 1. \tag{48}$$

To simplify our calculation, we consider $\mu \to \infty$ to enforce the normalization of the magnitude of spin at any position

in space and time: $\phi^2(x,t) \equiv 1$ [68]. In Fourier space, the latter implies that the formal solution can be written as,

$$\hat{\phi}_k(t)\hat{\phi}_l(t) = (2\pi)^{2d}\delta^d(k+l)W_k(t), \tag{49}$$

Here $W_k(t)$ should satisfy,

$$\int \mathrm{d}^d k\ W_k(t) = 1. \tag{50}$$

Note that $W_k(t)$ is the structure-factor of the projection field. The factor $\Gamma(t,t')$ (or equivalently $z(t)$) can be determined self-consistently so as to satisfy the normalization condition $\phi(x,t)^2 = 1$,

$$\Gamma(t,t') = \int \frac{\mathrm{d}^d k}{(2\pi)^d}\frac{\mathrm{d}^d l}{(2\pi)^d}\mathrm{e}^{-k^2(t-t')}\mathrm{e}^{-l^2(t-t')}\langle\hat{\phi}_k(t')\hat{\phi}_l(t')\rangle = \int \mathrm{d}^d k \mathrm{e}^{-2k^2(t-t')}W_k(t'). \tag{51}$$

Then the structure-factor (49) at time t is obtained formally as

$$W_k(t) = W_k(t')\frac{\mathrm{e}^{-2k^2(t-t')}}{\Gamma(t,t')}\cdot \tag{52}$$

4.1.4 Physical observables

The properties of coarsening systems can be well characterized using correlation functions. Given a structure-factor (49) at a certain time s, the auto-correlation function for two times $t > t' > s$ can be formally computed as,

$$C(r,t,t') = \langle\phi(r,t)\phi(0,t')\rangle = \int \mathrm{d}^d k \frac{\mathrm{e}^{-k^2((t-s)+(t'-s))}\mathrm{e}^{\mathrm{i}kr}W_k(s)}{\sqrt{\Gamma(t,s)}\sqrt{\Gamma(t',s)}}\cdot \tag{53}$$

In particular, the equal-time $t' = t$ spatial correlation function is obtained simple as the inverse Fourier transform in space of the structure factor $W_k(t)$,

$$C(r,t,t) = \int \mathrm{d}^d k \mathrm{e}^{\mathrm{i}kr}W_k(t). \tag{54}$$

Another important quantity is the local auto-correlation function,

$$C(r=0,t,t') = \frac{\Gamma((t+t')/2,s)}{\sqrt{\Gamma(t,s)}\sqrt{\Gamma(t',s)}}\cdot \tag{55}$$

In the following we denote the (local) auto-correlation function $C(r=0,t,t')$ as $C(t,t')$ for simplicity. Since coarsening is a non-stationary dynamics, the correlation functions depend not only on the time difference $t - t_\mathrm{w}$ but explicitly on the two times t and t_w. This feature is called 'waiting time effect' or 'violation of time translational invariance'.

In addition to the correlation functions, linear-response functions are also very interesting to study. In the spin-glass experiments, the measurement of the linear-response such as AC magnetic susceptibility is one of the only detailed probe for the dynamics. In Appendix C we present the formal solution for the linear-response function of the $O(n)$ Mattis model to uniform external field.

4.2 Standard coarsening

Before studying coarsening under cycling of equilibrium states, let us review some essential results in the case of standard coarsening, *i.e.* coarsening with un-biased random configuration with short-range correlation. The solution is well known and studied in detail [52].

Let us choose the random initial condition as,

$$\langle\hat{\phi}_k\hat{\phi}_l\rangle_\mathrm{ini} = \Delta(2\pi)^d\delta^d(k+l), \tag{56}$$

which is equivalent to

$$\langle\phi(x)\phi(x')\rangle_\mathrm{ini} = \Delta\delta^d(x-x'). \tag{57}$$

The latter means the structure-factor (49) is flat (white noise) at the beginning,

$$W_k(0) = \frac{\Delta}{(2\pi)^d}\cdot \tag{58}$$

Then the solution is obtained using (51) as,

$$\Gamma_0(t,0) = \frac{\Delta}{(2\pi)^d}\int \mathrm{d}^d k \mathrm{e}^{-2k^2 t} = \left(\frac{t}{\tau_0}\right)^{-d/2} \sim (L(t)/L_0)^{-2\lambda}, \tag{59}$$

where we defined a microscopic time scale $\tau_0 = \Delta^{2/d}/(8\pi)$. Note that this expression is valid for large enough time separation t compared with τ_0. In the limit $t = 0$ we must have the identity (48). For the definition of $L(t)$ and the exponent λ in the last equation see (61) and the following.

The correlation functions can be obtained using (54, 55, 58). The spatial correlation function at equal-time becomes,

$$C_0(r,t,t) = \langle\phi(r,t)\phi(0,t)\rangle = \frac{\Delta}{(2\pi)^d}\int \mathrm{d}^d k \frac{\mathrm{e}^{-2k^2 t}\mathrm{e}^{\mathrm{i}kr}}{\Gamma_0(t,0)} = \exp\left(-\frac{r^2}{8t}\right) \equiv \exp\left[-\left(\frac{r}{L(t)}\right)^2\right], \tag{60}$$

In the last equation we introduced a characteristic length scale,

$$L(t) \propto L_0\sqrt{t}, \tag{61}$$

where L_0 is some microscopic unit of length. Although there are no topological defects like domain walls in the spherical limit $n \to \infty$, the latter characteristic length scale plays the role of scaling variable as played by the mean separation of domain walls in the systems with domain walls [52].

The correlation between the random initial configuration and the temporary configuration at time t is obtained as

$$C_0(t,0) = \langle\phi^\beta(t)\phi^\beta(0)\rangle = \frac{\Gamma(t/2,0)}{\sqrt{\Gamma(t,0)}} = 2^{d/2}(t/\tau_0)^{-d/4} \sim (L(t)/L_0)^{-\lambda}. \tag{62}$$

The non-equilibrium dynamical exponent λ (see (14)) of the $O(n)$ model is known to be,

$$\lambda = d/2 \qquad O(n \to \infty) \text{ model}, \tag{63}$$

as one can see easily comparing with (61). More generally the two-time auto-correlation functions is obtained as,

$$C_0(t, t_{\rm w}) = \langle \phi^\beta(t)\phi^\beta(t_{\rm w})\rangle = \frac{\Gamma((t+t_{\rm w})/2, 0)}{\sqrt{\Gamma(t,0)}\sqrt{\Gamma(t_{\rm w},0)}} \sim_{t\gg t_{\rm w}} (L(t)/L(t_{\rm w}))^{-\lambda}. \tag{64}$$

Here the waiting time effect follows the $L(t)/L(t_{\rm w})$ type scaling behavior as in many other coarsening systems [52].

4.3 A cycle on a symmetry broken state

Let us now begin to analyze the effect of cycling the equilibrium states on coarsening with the simplest version described in Section 3.2.1. Here we look at how the projection of the temporary spin-configuration onto an equilibrium state is progressively affected by the coarsening of a completely unrelated phase. Subsequently we study in detail how the noise induced by this process can be removed progressively by performing the 'conjugate' coarsening.

4.3.1 Noise imprinting

Let us take a random ground state $\{\sigma_i^\alpha\}$ as the initial condition so that the symmetry is fully broken with respect to α at the beginning,

$$\hat{\phi}_k^\alpha(0) = (2\pi)^d \delta^d(k). \tag{65}$$

We then perform coarsening with respect to a completely unrelated ground state $\{\sigma_i^\beta\}$. The initial condition should look as a completely random configuration in the projection onto β. Due to (A.1) which is the Fourier transform of (38) we find,

$$\hat{\phi}_k^\beta(0) = \int \frac{{\rm d}^d k'}{(2\pi)^d} (\hat{\sigma}^{\alpha\beta})_{k'} (2\pi)^d \delta^d(k+k') = (\hat{\sigma}^{\alpha\beta})_k, \tag{66}$$

Here $(\hat{\sigma}^{\alpha\beta})_k$ is the transformation field defined in (A.2) which is a Gaussian random field (see Appendix A). By (A.3) and (A.4), one can check that the initial condition for the coarsening with respect to β is indeed a random initial condition with zero mean and short range correlation as it should. The solution of the equation of motion with such random initial condition is known as shown in (59).

Let us monitor the time evolution of the spin-configuration by projecting onto α through (A.1),

$$\hat{\phi}_k^\alpha(t) = \int \frac{{\rm d}^d k'}{(2\pi)^d} (\hat{\sigma}^{\alpha\beta})_{k'} \hat{\phi}_{k-k'}^\beta(t). \tag{67}$$

Using the 2-body correlation function of $(\hat{\sigma}^{\alpha\beta})_k$ shown in (A.4), one finds that the resultant configuration have the following properties.

First, it is easy to see that the $k = 0$ component of the projection onto α has non-zero mean while the others have zero mean,

$$\langle \hat{\phi}_k^\alpha(t)\rangle_\sigma = (2\pi)^d \delta^d(k)\ \rho \tag{68}$$

or

$$\langle \hat{\phi}^\alpha(x,t)\rangle_\sigma = \rho \tag{69}$$

with

$$\rho = C_0(t,0) \sim (L(t)/L_0)^{-\lambda}. \tag{70}$$

The result means that the symmetry remains broken with a weaker and weaker bias ρ as the coarsening time t with respect the unrelated phase β increase. This feature has been discussed in Section 3.2.1 (see (15)).

Second, the spatial correlation of the projection to α can also be obtained as described in Appendix B. The initial condition (65) implies that initial structure-factor is $W_k^\alpha(0) = \delta^d(k)$ in (49). Then from (B.12), we obtain the correlation function as,

$$\langle \hat{\phi}_k^\alpha(t)\hat{\phi}_l^\alpha(t)\rangle_\sigma = (2\pi)^{2d}\delta^d(k+l) W_k^\alpha(t), \tag{71}$$

with the structure-factor,

$$W_k^\alpha(t) = \rho^2 \delta^d(k) + \frac{\Delta}{(2\pi)^d}(1 - 2\rho^2 + {\rm e}^{-k^2 t/2}). \tag{72}$$

By taking the inverse Fourier transform one finds[3],

$$\langle \phi^\alpha(x,t)\phi^\alpha(x',t)\rangle_\sigma - \langle \phi^\alpha(x,t)\rangle_\sigma \langle \phi^\alpha(x',t)\rangle_\sigma = \Delta\delta^d(x-x')[1-2\rho^2] + {\rm e}^{-(x-x')/2t}\rho^2. \tag{73}$$

To summarize, coarsening of unrelated phase produces essentially short-ranged correlated random field with weak bias as we expected in Section 3.2.1.

4.3.2 Noise cleaning

Let us stop the coarsening of the unrelated phase β at time $t = t_{\rm w2}$ and see closely how the noise imprinted on the projection field to α is removed by coarsening with respect to α for some additional time $t_{\rm w3}$. Given $\phi^\alpha(x, t_{\rm w2})$ obtained in the last stage as the initial condition for this stage, the solution at time $t_{\rm w3} + t_{\rm w2}$ is obtained as

$$\hat{\phi}_k^\alpha(t_{\rm w3} + t_{\rm w2}) = \hat{\phi}_k^\alpha(t_{\rm w2}) \frac{{\rm e}^{-k^2 t_{\rm w3}}}{\sqrt{\Gamma_{\rm cycle}(t_{\rm w3}+t_{\rm w2}, t_{\rm w2})}}. \tag{74}$$

[3] In the derivation of the last equation we used $\Gamma(t/4, 0) = C^2(t,0) = \rho^2$ as one can check from (62) and (59).

Here the factor $\mathit{\Gamma}_{\rm cycle}(t_{\rm w3}+t_{\rm w2},t_{\rm w2})$ is obtained using (51, 72) and (59) as[4],

$$\mathit{\Gamma}_{\rm cycle}(t_{\rm w3}+t_{\rm w2},t_{\rm w2})=\rho^2+(1-2\rho^2)\mathit{\Gamma}_0(t_{\rm w3},0)+\mathit{\Gamma}_0(t_{\rm w3}+t_{\rm w2}/4,0),\quad(75)$$

with

$$\rho=C_0(t_{\rm w2},0)\sim(L(t_{\rm w2})/L_0)^{-\lambda}.\quad(76)$$

Here $\mathit{\Gamma}_0$ is the one obtained in the solution for standard coarsening (59) with un-biased random initial condition.

For the following analysis, it is useful to introduce the relative ratios of the three terms in (75), which will find a natural interpretation later:

$$m^2_{\rm mem}(t_{\rm w3},t_{\rm w2})=\rho^2/\mathit{\Gamma}_{\rm cycle}(t_{\rm w3}+t_{\rm w2},t_{\rm w2}),\quad(77)$$

$$m^2_{\rm rej}(t_{\rm w3},t_{\rm w2})=(1-2\rho^2)\mathit{\Gamma}_0(t_{\rm w3},0)/\mathit{\Gamma}_{\rm cycle}(t_{\rm w3}+t_{\rm w2},t_{\rm w2}),\quad(78)$$

$$\tilde{m}^2(t_{\rm w3},t_{\rm w2})=\mathit{\Gamma}_0(t_{\rm w3}+t_{\rm w2}/4,0)/\mathit{\Gamma}_{\rm cycle}(t_{\rm w3}+t_{\rm w2},t_{\rm w2}).\quad(79)$$

By definition the sum of the three is always 1.

Suppose that $t_{\rm w2}$ has been chosen to sufficiently large. Then for small enough $t_{\rm w3}$ compared with $t_{\rm w2}$, $m_{\rm rej}$ is dominant,

$$m^2_{\rm rej}\simeq 1\qquad\text{or}\qquad \mathit{\Gamma}_{\rm cycle}(t_{\rm w3}+t_{\rm w2},t_{\rm w2})\simeq\mathit{\Gamma}_0(t_{\rm w3},0)\sim(L(t_{\rm w3})/L_0)^{-2\lambda}\quad t_{\rm w3}\ll\tau_{\rm rec}.\quad(80)$$

here we used (59). On the other hand, at large enough time $t_{\rm w3}$, $m_{\rm rej}$ and $\tilde{m}^2$ go to zero,

$$m^2_{\rm mem}\simeq 1\qquad\text{or}\qquad \mathit{\Gamma}_{\rm cycle}(t_{\rm w3}+t_{\rm w2},t_{\rm w2})\simeq\rho^2 t_{\rm w3}\gg\tau_{\rm rec}.\quad(81)$$

The crossover between the two limits takes place when the ratio $m^2_{\rm rej}$ and $m^2_{\rm mem}$ becomes of the same order (we are assuming $\tilde{m}^2\ll m^2_{\rm rej}$). Then using (59) one finds the crossover time $\tau_{\rm rec}(\rho)$ as,

$$\rho\sim(L(\tau_{\rm rec}(\rho))/L_0)^{-\lambda}.\quad(82)$$

The above feature has direct consequences on the physical observables.

First, let us consider the density of staggered magnetization. Using (68), it is obtained simply as,

$$\langle\phi^\alpha(t_{\rm w3}+t_{\rm w2})\rangle_\sigma=\int\frac{{\rm d}^dk}{(2\pi)^d}\frac{{\rm e}^{-k^2t_{\rm w3}}}{\sqrt{\mathit{\Gamma}_{\rm cycle}(t_{\rm w3}+t_{\rm w2},t_{\rm w2})}}\langle\phi^\alpha_k(t_{\rm w2})\rangle_\sigma=\frac{\rho}{\sqrt{\mathit{\Gamma}_{\rm cycle}(t_{\rm w3}+t_{\rm w2},t_{\rm w2})}}=m_{\rm mem}(t_{\rm w3},t_{\rm w2}).\quad(83)$$

[4] One can check that $\mathit{\Gamma}(t_{\rm w2},t_{\rm w2})=1$ is satisfied since $\mathit{\Gamma}(t_{\rm w2}/4)=C^2(t_{\rm w2},0)=\rho^2$ as one can check and $\mathit{\Gamma}_0(0,0)=1$ because of the identity (48).

In the last equation we used the definition of $m^2_{\rm mem}(t_{\rm w3},t_{\rm w2})$ given in (77). Thus $m_{\rm mem}(t_{\rm w3},t_{\rm w2})$ is the staggered magnetization in the bulk, that will contribute to the memory effect. The staggered magnetization starts from ρ and saturates to the full moment 1 at time scales large enough compared with $\tau_{\rm rec}(\rho)$ defined in (82). It means that the density of the minority phase shrinks and the fully symmetry broken state is almost recovered within a finite time scale.

Second, let us consider the equal time spatial correlation function of fluctuation of the projected field around the mean $\langle\phi^\alpha(t_{\rm w3}+t_{\rm w2})\rangle_\sigma$,

$$\delta\phi^\alpha(r,t_{\rm w3}+t_{\rm w2})=\phi^\alpha(r,t_{\rm w3}+t_{\rm w2})-\langle\phi^\alpha(t_{\rm w3}+t_{\rm w2})\rangle_\sigma.\quad(84)$$

Using (54, 52, 75) and (72) and (83) it is obtained as,

$$\langle\delta\phi^\alpha(r,t_{\rm w3}+t_{\rm w2})\delta\phi^\alpha(0,t_{\rm w3}+t_{\rm w2})\rangle_\sigma=\int{\rm d}^dk\left[\frac{\mathit{\Delta}}{(2\pi)^d}\left(1-2\rho^2+{\rm e}^{-k^2t_{\rm w2}/2}\right)\right]\times\frac{{\rm e}^{-2k^2t_{\rm w3}}}{\mathit{\Gamma}_{\rm cycle}(t_{\rm w3}+t_{\rm w2},t_{\rm w2})}=m^2_{\rm rej}(t_{\rm w3},t_{\rm w2})\exp\left(-\frac{r^2}{8t_{\rm w3}}\right)+\tilde{m}^2(t_{\rm w3},t_{\rm w2})\exp\left(-\frac{r^2}{8(t_{\rm w3}+t_{\rm w2}/4)}\right).\quad(85)$$

In the last equation we used the parameters defined in (78) and (79). This result should be compared with the case of coarsening with un-biased initial condition (60). For simplicity we assume that $t_{\rm w2}$ has been taken very large so that the second term can be neglected. Then one finds that at short enough time scale the amplitude of the correlation function stays constant $m^2_{\rm rej}\simeq 1$ because of (80). In this regime the behavior of the correlation function is essentially the same as in the usual case of coarsening with un-biased initial condition (60); this contribution will therefore be associated to rejuvenation. The range of correlation grows as,

$$\langle\delta\phi^\alpha(r,t_{\rm w3}+t_{\rm w2})\delta\phi^\alpha(0,t_{\rm w3}+t_{\rm w2})\rangle_\sigma\simeq\exp\left[-\left(\frac{r}{L(t_{\rm w3})}\right)^2\right]\qquad t_{\rm w3}\ll\tau_{\rm rec}.\quad(86)$$

At larger time scale compared with $\tau_{\rm rec}$, the amplitude $m^2_{\rm rej}$ vanishes because of (81) and the fluctuation disappears, *i.e.* the system is ordered again,

$$\langle\delta\phi^\alpha(r,t_{\rm w3}+t_{\rm w2})\delta\phi^\alpha(0,t_{\rm w3}+t_{\rm w2})\rangle_\sigma\simeq 0\qquad t_{\rm w3}\gg\tau_{\rm rec}.\quad(87)$$

Finally let us consider the auto-correlation functions. The simplest one which is useful is the correlation between the configuration at the beginning of the final coarsening with that at some later time. One easily obtains,

$$C(t_{\rm w3}+t_{\rm w2},t_{\rm w2})=\frac{\mathit{\Gamma}_{\rm cycle}(t_{\rm w3}/2+t_{\rm w2},t_{\rm w2})}{\sqrt{\mathit{\Gamma}_{\rm cycle}(t_{\rm w3}+t_{\rm w2},t_{\rm w2})}}\cdot\quad(88)$$

This result should be compared with the case with zero bias (62). One can easily see that at the beginning $t_{\rm w3} \ll \tau_{\rm rec}$ where $\Gamma_{\rm cycle}(t_{\rm w3}+t_{\rm w2}, t_{\rm w2}) \simeq \Gamma_0(t_{\rm w3}, 0)$ (80) holds, the correlation function decreases as if starting from random initial conditions without bias,

$$C(t_{\rm w3}+t_{\rm w2}, t_{\rm w2}) \simeq C_0(t_{\rm w3}, 0) \sim (L(t_{\rm w3})/L_0)^{-\lambda} \qquad t_{\rm w3} \ll \tau_{\rm rec}. \quad (89)$$

On the other hand it saturates at large enough time scales due to $\Gamma_{\rm cycle}(t_{\rm w3}+t_{\rm w2}, t_{\rm w2}) \simeq \rho^2$, see (81), as

$$C(t_{\rm w3}+t_{\rm w2}, t_{\rm w2}) = \rho \qquad t_{\rm w3} \gg \tau_{\rm rec}. \quad (90)$$

In Section 3.2.1, we expected this feature on general grounds and used it to estimate the recovery time (16).

4.4 Double coarsening in one step cycling

Now we analyze the double coarsening process discussed in Section 3.3 in the present specific model. We first let the system coarsen towards the equilibrium state α for time $t_{\rm w1}$ starting from a random initial condition (56). Then we change the target state to β for a time $t_{\rm w2}$, given the configuration obtained above as the initial configuration. And finally, we switch back the coarsening towards the original equilibrium state α for time $t_{\rm w3}$. Note that the process we considered in the previous subsection can be regarded as the special case of $t_{\rm w1} = \infty$.

4.4.1 The first and second coarsening

The first stage is the usual coarsening from random initial conditions. The structure-factor of the projection field with respect to α after time $t_{\rm w1}$ is given in (58) which reads,

$$W_k^\alpha(t_{\rm w1}) = \frac{\Delta}{(2\pi)^d} \frac{{\rm e}^{-2k^2 t_{\rm w1}}}{\Gamma_0(t_{\rm w1}, 0)}\,. \quad (91)$$

As we discuss in Appendix B, the projection of this configuration onto β is random with zero mean (B.7) and short range correlation (B.8). Thus a new coarsening process begins in the second stage. After time $t_{\rm w2}$, the correlation with the configuration at time $t_{\rm w1}$ is,

$$\rho = C(t_{\rm w2}, 0) \sim (L(t_{\rm w2})/L_0)^{-\lambda}. \quad (92)$$

In the following we analyze the time evolution of the coarsening in the second stage (towards β) by projecting onto α. The basic information is the structure-factor of the projection field with respect to α which can be obtained using (B.11) and (91),

$$\begin{aligned} W_k^\alpha(t_{\rm w2}+t_{\rm w1}) &= \rho^2 W_k^\alpha(t_{\rm w1}) + \frac{\Delta}{(2\pi)^d} \\ &\times \Bigg[1 - 2\rho^2 \frac{1}{\Gamma_0(t_{\rm w2}, 0)} \frac{\Delta}{(2\pi)^d} \int {\rm d}^d k' \\ &\times \int {\rm d}^d l' {\rm e}^{-(k-k')^2 t_{\rm w2}} {\rm e}^{-(k+l')^2 t_{\rm w2}} \\ &\times W^\alpha_{k-k'+l}(t_{\rm w1})\Bigg] \\ &= \rho^2 \frac{\Delta}{(2\pi)^d} \frac{{\rm e}^{-2k^2 t_{\rm w1}}}{\Gamma_0(t_{\rm w1}, 0)} + \frac{\Delta}{(2\pi)^d}(1-2\rho^2) \\ &+ \rho^2 \frac{\Delta}{(2\pi\sqrt{A(t_{\rm w1}/t_{\rm w2})})^d} \\ &\times \frac{\exp\left(-2k^2 t_{\rm w1}/A(t_{\rm w1}/t_{\rm w2})\right)}{\Gamma_0(t_{\rm w1}, 0)}\,. \end{aligned} \quad (93)$$

where

$$A(y) \equiv 1 + 4y. \quad (94)$$

The spatial correlation function of the projection with respect to α is obtained immediately using (93) in (54) as,

$$\begin{aligned} &C(r, t_{\rm w2}+t_{\rm w1}, t_{\rm w2}+t_{\rm w1}) = \\ &\qquad \rho^2 \exp\left(-\frac{r^2}{8t_{\rm w1}}\right) + (1-2\rho^2)\Delta\delta^d(r) \\ &+ \rho^2 A^{-d/2}(t_{\rm w1}/t_{\rm w2}) \exp\left(-\frac{r^2}{8t_{\rm w1}/A(t_{\rm w1}/t_{\rm w2})}\right). \end{aligned} \quad (95)$$

This simple result immediately allows its physical interpretation. The first term in (95) can be written as $\rho^2 \exp(-(r/L(t_{\rm w1}))^2)$ which implies the remnant of the spatial correlation established in the first stage. The amplitude ρ decreases as (92) in the second stage. This can be interpreted as the correlation between the 'ghost' domains discussed in Section 3.3 which is losing its amplitude. Thus no matter how large the noise becomes, the 'memory' of the spatial structure is conserved. The second term (95) represent the short-range noise induced by the coarsening of an unrelated phase. The last term becomes the same as the first term in the limit $L(t_{\rm w2}) \gg L(t_{\rm w1})$ since $A \simeq 1$ as one can see from (94). In the other limit, $L(t_{\rm w1}) \gg L(t_{\rm w2})$, it can be neglected.

4.4.2 Inner- and outer-coarsening regimes in the third stage

We now restore the equilibrium state α as the target state for time $t_{\rm w3}$ given the 'noisy' spin-configuration at the end of the second stage as the input. Here we examine the scenario conjectured in Section 3.3 that the inner-coarsening transforms the 'ghost domains' back into 'real domains'. We demonstrate that the inner-coarsening regime, the intermediate plateau regime and the outer-coarsening regime show up explicitly in various correlation functions and response functions.

Using (93) in (51), the Γ factor in the third stage which we denote as $\Gamma_{1-\mathrm{step}}$ is obtained as,

$$\Gamma_{1-\mathrm{step}}(t_{\mathrm{w}3}+t_{\mathrm{w}2}+t_{\mathrm{w}1},t_{\mathrm{w}2}+t_{\mathrm{w}1}) = \int \mathrm{d}^d k \mathrm{e}^{-2k^2 t_{\mathrm{w}3}} W_k^\alpha(t_{\mathrm{w}2}+t_{\mathrm{w}1}) = \rho^2\Gamma_0(t_{\mathrm{w}3}+t_{\mathrm{w}1},t_{\mathrm{w}1}) + (1-2\rho^2)\Gamma_0(t_{\mathrm{w}3},0) + \rho^2 A^{-d/2}(t_{\mathrm{w}1}/t_{\mathrm{w}2})\Gamma_0\left(t_{\mathrm{w}3}+\frac{t_{\mathrm{w}1}}{A(t_{\mathrm{w}1}/t_{\mathrm{w}2})},t_{\mathrm{w}1}\right). \quad (96)$$

Here Γ_0 is the one obtained in the solution for standard coarsening (59) with un-biased random initial condition. It is again useful to define the relative ratio of the contribution of the three terms in the last equation as,

$$m^2_{\mathrm{mem}}(t_{\mathrm{w}3},t_{\mathrm{w}2},t_{\mathrm{w}1}) = \rho^2\Gamma_0(t_{\mathrm{w}3}+t_{\mathrm{w}1},t_{\mathrm{w}1})/\Gamma_{1-\mathrm{step}}(t_{\mathrm{w}3}+t_{\mathrm{w}2}+t_{\mathrm{w}1},t_{\mathrm{w}2}+t_{\mathrm{w}1}), \quad (97)$$

$$m^2_{\mathrm{rej}}(t_{\mathrm{w}3},t_{\mathrm{w}2},t_{\mathrm{w}1}) = (1-2\rho^2)\Gamma_0(t_{\mathrm{w}3},0)/\Gamma_{1-\mathrm{step}}(t_{\mathrm{w}3}+t_{\mathrm{w}2}+t_{\mathrm{w}1},t_{\mathrm{w}2}+t_{\mathrm{w}1}), \quad (98)$$

$$\tilde{m}^2(t_{\mathrm{w}3},t_{\mathrm{w}2},t_{\mathrm{w}1}) = \rho^2 A^{-d/2}(t_{\mathrm{w}1}/t_{\mathrm{w}2})\Gamma_0 \times \left(t_{\mathrm{w}3}+\frac{t_{\mathrm{w}1}}{A(t_{\mathrm{w}1}/t_{\mathrm{w}2})},t_{\mathrm{w}1}\right)/\Gamma_{1-\mathrm{step}} \times (t_{\mathrm{w}3}+t_{\mathrm{w}2}+t_{\mathrm{w}1},t_{\mathrm{w}2}+t_{\mathrm{w}1}). \quad (99)$$

The structure-factor of the projected field to α is obtained using (52) as,

$$W_k^\alpha(t_{\mathrm{w}3}+t_{\mathrm{w}2}+t_{\mathrm{w}1}) = W_k^\alpha(t_{\mathrm{w}2}+t_{\mathrm{w}1})\frac{\mathrm{e}^{-2k^2 t_{\mathrm{w}3}}}{\Gamma_{1-\mathrm{step}}(t_{\mathrm{w}3}+t_{\mathrm{w}2}+t_{\mathrm{w}1},t_{\mathrm{w}2}+t_{\mathrm{w}1})}, \quad (100)$$

where $W_k^\alpha(t_{\mathrm{w}2}+t_{\mathrm{w}1})$ is given in (93) and $\Gamma_{1-\mathrm{step}}(t_{\mathrm{w}3}+t_{\mathrm{w}2}+t_{\mathrm{w}1},t_{\mathrm{w}2}+t_{\mathrm{w}1})$ is given in (96). Then the spatial correlation function of the projected field is obtained using (100, 93) and (96) in (54) as,

$$C(r,t_{\mathrm{w}3}+t_{\mathrm{w}2}+t_{\mathrm{w}1},t_{\mathrm{w}3}+t_{\mathrm{w}2}+t_{\mathrm{w}1}) = m^2_{\mathrm{mem}}(t_{\mathrm{w}3},t_{\mathrm{w}2},t_{\mathrm{w}1})\exp\left(-\frac{r^2}{8(t_{\mathrm{w}3}+t_{\mathrm{w}1})}\right) + m^2_{\mathrm{rej}}(t_{\mathrm{w}3},t_{\mathrm{w}2},t_{\mathrm{w}1})\exp\left(-\frac{r^2}{8t_{\mathrm{w}3}}\right) + \tilde{m}^2(t_{\mathrm{w}3},t_{\mathrm{w}2},t_{\mathrm{w}1})\exp\left(-\frac{r^2}{8(t_{\mathrm{w}3}+t_{\mathrm{w}1}/A(t_{\mathrm{w}1}/t_{\mathrm{w}2}))}\right). \quad (101)$$

In the last equation we used the parameters introduced in (97, 98) and (99). Note that there is a sum rule,

$$m^2_{\mathrm{mem}} + m^2_{\mathrm{rej}} + \tilde{m}^2 = 1, \quad (102)$$

by the definition of the parameters. Obviously the first term in (101) can be physically understood as the correlation due to the continuation of the 'ghost domains' (memory). The amplitude m_{mem} can be regarded as the staggered magnetization associated with the continuation of the 'ghost domains'. Similarly the second term can be interpreted as the correlation due to re-start of coarsening within the ghost domains (rejuvenation), which we called 'inner-coarsening' in Section 3.3. The role of the last term depends on relative ratio of the size of the domains in the first and second regime as we discuss later.

Now we discuss the change of the profile of the spatial correlation function with increasing time $t_{\mathrm{w}3}$ in the third stage. We assume that the duration of the second regime is large enough so that the bias has become very small $\rho \ll 1$. Then at the beginning for small $t_{\mathrm{w}3}$, we find the parameter defined in (98) is $m^2_{\mathrm{rej}} \simeq 1$ while the other two m^2_{mem} and $\tilde{m}^2$ defined in (97) and (99) are very small. Then the second term in (101) which represent the inner-coarsening (rejuvenation) is therefore dominant,

$$C(r,t_{\mathrm{w}3}+t_{\mathrm{w}2}+t_{\mathrm{w}1},t_{\mathrm{w}3}+t_{\mathrm{w}2}+t_{\mathrm{w}1}) \simeq \exp\left[-\left(\frac{r}{L(t_{\mathrm{w}3})}\right)^2\right] \quad \text{inner-coarsening regime} \quad (103)$$

On the other hand, in the asymptotically large time scale such that $L(t_{\mathrm{w}3}) \sim L(t_{\mathrm{w}3}+t_{\mathrm{w}1})$, (*i.e.* $t_{\mathrm{w}3} \sim t_{\mathrm{w}1}$), the spatial correlation function becomes,

$$C(r,t_{\mathrm{w}3}+t_{\mathrm{w}2}+t_{\mathrm{w}1},t_{\mathrm{w}3}+t_{\mathrm{w}2}+t_{\mathrm{w}1}) \simeq \exp\left[-\left(\frac{r}{L(t_{\mathrm{w}3}+t_{\mathrm{w}1})}\right)^2\right], \quad \text{outer-coarsening regime} \quad (104)$$

Here we used the sum rule (102). This regime can be interpreted as the outer coarsening regime we discussed in Section 3.3.

We have discussed in Section 3.3 that the crossover between the inner-coarsening and outer-coarsening regime depends on the relative domain sizes of the first and second stages. We will indeed find below that it is the case in the present model. In the following we consider the two limiting cases: a) $L(t_{\mathrm{w}1}) \gg L(t_{\mathrm{w}2})$ and b) $L(t_{\mathrm{w}1}) \ll L(t_{\mathrm{w}2})$.

4.4.3 Rejuvenation and memory: Case a)

We consider the case a) $L(t_{\mathrm{w}1}) \gg L(t_{\mathrm{w}2})$: the duration of the first stage is much longer than the second. In this case the parameter $\tilde{m}^2$ is very small compared with m^2_{rej} since $A \gg 1$ as one can see in (94). Thus we neglect the last term in the spatial correlation function given in (101). Then the basic structure of the correlation function (101) can be naturally interpreted as a sum of Gaussian packet due to the inner-coarsening (rejuvenation) whose size is $L(t_{\mathrm{w}3})$ (second term) and that due to the continuation of the 'ghost domains' (memory) of size $L(t_{\mathrm{w}3}+t_{\mathrm{w}1})$ (first term). In this case, the inner-coarsening regime (103) terminates due to the effect of the bias as we discussed in

Section 3.3. Furthermore there is an intermediate regime which we called 'plateau regime' in Section 3.3 so that rejuvenation and memory effects can be observed in a well separated manner.

Let us consider the characteristic time scale at which the staggered magnetization of the ghost domain $m_{\rm mem}$ defined in (97) and $m_{\rm rej}$ defined in (98) become the same order. For short times such that $L(t_{\rm w3}) \ll L(t_{\rm w1})$, we can assume $\Gamma_0(t_{\rm w3}+t_{\rm w1}, t_{\rm w1}) \sim 1$ in (97). Then the time scale $\tau_{\rm rec}(\rho)$ at which $m_{\rm mem}$ and $m_{\rm rej}$ become the same order is obtained using (59) as,

$$\rho \sim (L(\tau_{\rm rec}(\rho)/L_0)^{-\lambda}, \tag{105}$$

which is the same as (82) obtained in the limit $L(t_{\rm w1}) \to \infty$. Note that the assumption $\Gamma_0(t_{\rm w1}+t_{\rm w3}, t_{\rm w1}) \sim 1$ is still satisfied because the bias is $\rho \sim (L(t_{\rm w2})/L_0)^{-\lambda}$ as given in (92) which implies

$$L(\tau_{\rm rec}(\rho)) \ll L(t_{\rm w1}). \tag{106}$$

When the inner-coarsening regime ends, we are left with the 'ghost domains' which have *almost* recovered their full staggered magnetization $m_{\rm mem} \simeq 1$. The latter can be interpreted as the fact that the 'real domain' are recovered. However, the relation (106) implies that the relaxation time $\tau_{\rm rec}(\rho)$ is not large enough to grow the revived domain further. Thus there is an intermediate regime where:

$$C(r, t_{\rm w3}+t_{\rm w2}+t_{\rm w1}, t_{\rm w3}+t_{\rm w2}+t_{\rm w1}) \simeq \exp\left[-\left(\frac{r}{L(t_{\rm w1})}\right)^2\right],$$

$$\text{plateau regime} \quad L(t_{\rm w1}) \gg L(t_{\rm w3}) \gg L(\tau_{\rm rec}(\rho)). \tag{107}$$

This is the plateau regime in which the revived domain appears frozen in time. Thus the memory (spatial structure of bias) conserved in the system is retrieved with its original full amplitude within this regime. Much later in time, the plateau regime is followed by the asymptotic outer-coarsening regime (104).

4.4.4 Complete rejuvenation: Case b)

Next we discuss the case b) $L(t_{\rm w1}) \ll L(t_{\rm w2})$: the duration of the first stage is much shorter than that of the second stage. In this case we find that the two contributions defined in (98) and (99) become essentially equal $m_{\rm mem}^2 \simeq \tilde{m}^2$ since $A \simeq 1$ holds as one can see in (94). Thus the basic structure of the correlation function (101) can be again naturally interpreted as a sum of Gaussian packet due to the domain of inner-coarsening (rejuvenation) whose size is $L(t_{\rm w3})$ and that due to the continuation of the 'ghost domain' (memory) of size $L(t_{\rm w3}+t_{\rm w1})$.

However, the amplitude of the memory terms $m_{\rm mem}^2 (\simeq \tilde{m}^2)$ does not recover much and saturates to a small value $\sim (L(t_{\rm w1})/L(t_{\rm w2}))^{\lambda} \ll 1$ as $L(t_{\rm w3}) \sim L(t_{\rm w1})$ ($t_{\rm w3} \sim t_{\rm w1}$). In the latter regime, the width of the memory and rejuvenation terms become of the same order,

$$L(t_{\rm w3}) \sim L(t_{\rm w1}+t_{\rm w3}); \qquad t_{\rm w3} \sim t_{\rm w1} \tag{108}$$

Thus the correlation function crossovers very smoothly to the asymptotic outer-coarsening regime (104) so that the memory cannot be retrieved. The resultant behavior of the correlation function is not very different from the case of $t_{\rm w} = 0$. In this sense the relaxation is almost completely rejuvenated.

4.4.5 U-turn in the phase space

The above result implies the time evolution of system in the phase space during the third stage is such that it makes an U-turn to configuration before the second stage (inner-coarsening) and stay there for a while (plateau-regime) and finally make further excursion (outer-coarsening). Such a feature can be elucidated by considering overlap q between the configuration just after the first stage and the temporal configuration in the third stage. It is readily obtained as,

$$\begin{aligned} q(t_{\rm w3}) &= \int \frac{{\rm d}^d k}{(2\pi)^d} \int \frac{{\rm d}^d l}{(2\pi)^d} \langle \langle \phi_k(t_{\rm w3}+t_{\rm w2}+t_{\rm w1}) \rangle_\sigma \\ &\quad \times \phi_l(t_{\rm w1}) \rangle_{\rm ini} \\ &= \int {\rm d}^d k \frac{\rho {\rm e}^{-k^2 t_{\rm w3}}}{\sqrt{\Gamma_{1-{\rm step}}(t_{\rm w3}+t_{\rm w2}+t_{\rm w1}, t_{\rm w2}+t_{\rm w1})}} \\ W_k^{\alpha}(t_{\rm w1}) &= \frac{\rho \Gamma_{1-{\rm step}}((t_{\rm w3}+t_{\rm w1}+t_{\rm w1})/2, t_{\rm w2})}{\sqrt{\Gamma_{1-{\rm step}}(t_{\rm w3}+t_{\rm w2}+t_{\rm w1}, t_{\rm w2}+t_{\rm w1})}} \\ &= C_0(t_{\rm w3}+t_{\rm w1}, t_{\rm w1}) m_{\rm mem}(t_{\rm w3}, t_{\rm w2}, t_{\rm w1}). \end{aligned} \tag{109}$$

In the last equation we used the ratio $m_{\rm mem}$ defined in (97) and C_0 is the auto-correlation function of standard coarsening (62).

As we found in the previous sections the ratio $m_{\rm mem}(t_{\rm w3}, t_{\rm w2}, t_{\rm w1})$ can be physically understood as the staggered magnetization which increases with $t_{\rm w3}$ in the third stage. On the other hand, the factor $C_0(t_{\rm w3}+t_{\rm w1}, t_{\rm w1})$ which appears in (109) describes de-correlation due to outer-coarsening.

The competing effects of the inner-coarsening and outer-coarsening make the overlap $q(t_{\rm w3})$ non-monotonic in time $t_{\rm w3}$. In the case a) $L(t_{\rm w1}) \gg L(t_{\rm w2})$ the behavior is the following. It *increases* during the inner-coarsening because of the increase of $m_{\rm mem}$ and almost saturate to 1 at time scale $t_{\rm w3}$ at around the recovery time $\tau_{\rm rec}(\rho)$. It stays close to 1 during plateau regime. Then in the outer-coarsening regime, it *decreases* with time. This picture obviously becomes invalid in the case of b) $L(t_{\rm w1}) \ll L(t_{\rm w2})$.

4.5 Three-stage relaxation of auto-correlation function after one-step cycling

We now turn to more conventional observables with which the rejuvenation and memory effects can be see easily.

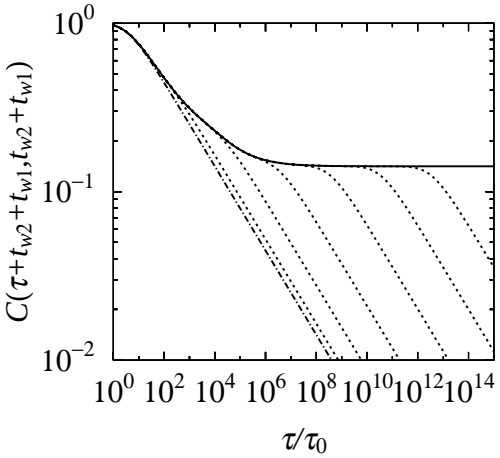

Fig. 6. The auto-correlation function $C(\tau+t_{\rm w2}+t_{\rm w1}, t_{\rm w2}+t_{\rm w1})$ in the $O(n)$ Mattis model ($d=1$) under one-step cycling. The dotted lines are curves with common $t_{\rm w2}=10^4$ but varying $t_{\rm w1}=10^2, 10^4, 10^6, 10^8, 10^{10}, 10^{12}$ (from left to right). The solid line on the top is the curve with $t_{\rm w2}=10^4$ but with $t_{\rm w1}=\infty$ (top). The dash-dotted line is the reference curve with zero waiting time of standard coarsening $C_0(\tau,0)$ (left most).

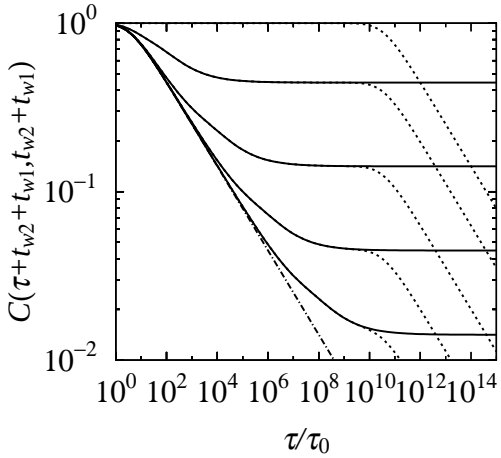

Fig. 7. The auto-correlation function $C(\tau+t_{\rm w2}+t_{\rm w1}, t_{\rm w2}+t_{\rm w1})$ in the $O(n)$ Mattis model ($d=1$) under one-step cycling. The dotted lines are curves with common $t_{\rm w1}=10^{10}$ but varying $t_{\rm w2}=0, 10^2, 10^4, 10^6, 10^8$ (from top to bottom). The solid lines are the reference curve of $t_{\rm w1}=\infty$ but varying $t_{\rm w2}=10^2, 10^4, 10^6, 10^8$ (from top to bottom). The dash-dotted line is the reference curve of zero waiting time of standard coarsening $C_0(\tau,0)$.

While the spatial correlation function of the projection field discussed above is convenient for theoretical discussions, it is obviously impractical in simulations and experiments of spin-glasses. In this section, we consider auto-correlation functions and linear response functions in the next section. These quantities are invariant under changes of projections and can be measured directly in numerical simulations and experiments. We will demonstrate that the characteristic three-stage relaxation after one-step cycling: inner-coarsening (rejuvenation), plateau and outer-coarsening (memory) regimes show up explicitly in these two-time quantities.

The auto-correlation function between two times in the third stage is obtained using (96) in (55) as,

$$C(\tau+t_{\rm w}^{\rm total}, t_{\rm w}^{\rm total}) = \frac{\Gamma_{1-\rm step}(\tau/2+t_{\rm w}^{\rm total}, t_{\rm w2}+t_{\rm w1})}{\sqrt{\Gamma_{1-\rm step}(\tau+t_{\rm w}^{\rm total}, t_{\rm w2}+t_{\rm w1})}\sqrt{\Gamma_{1-\rm step}(t_{\rm w}^{\rm total}, t_{\rm w2}+t_{\rm w1})}} \tag{110}$$

with
$$t_{\rm w}^{\rm total} \equiv t_{\rm w3}+t_{\rm w2}+t_{\rm w1}. \tag{111}$$

Here the explicit form of the Γ-factor is given in (96). As we discussed in Section 3.5, the auto correlation function can be related with the DC-magnetic susceptibilities measured in experiments.

First, let us look at the simplest case $t_{\rm w3}=0$: *i.e.* the correlation between the configuration just at the beginning of the third stage and the configuration a time τ later. Here we only consider the case a) $L(t_{\rm w1}) \gg L(t_{\rm w2})$ which allows clear separation between the inner- and outer-coarsening regimes. Within the inner-coarsening regime $\tau \ll \tau_{\rm rec}$ the amplitude of the ghost domains is small $m_{\rm mem} \ll 1$ and $m_{\rm rej} \simeq 1$. When the inner-coarsening ends at $\tau \sim \tau_{\rm rec}$, the amplitude of the ghost domains is almost recovered: $m_{\rm mem} \simeq 1$ and $m_{\rm rej} \ll 1$. Then one can see easily that the correlation function have the following feature,

$$C(\tau+t_{\rm w2}+t_{\rm w1}, t_{\rm w2}+t_{\rm w1}) = \begin{cases} C_0(\tau,0) & L(\tau) \ll L(\tau_{\rm rec}(\rho)) \quad (112) \\ \rho C_0(\tau+t_{\rm w1}, t_{\rm w1}) & L(\tau) \gg L(\tau_{\rm rec}(\rho)). \quad (113) \end{cases}$$

Here C_0 is the auto-correlation function in the standard coarsening given in (109). The result confirms the scaling property (30) conjectured in Section 3.5. It visualizes clearly the cross-over from inner-coarsening, plateau regime and outer-coarsening. Note that in the limit $L(t_{\rm w1}) \to \infty$, the last relaxation does not occur $C_0(\tau+t_{\rm w1}, t_{\rm w1})=1$ and we recover the result of the case in which we start from fully symmetry broken state with respect to phase α. (see (89) and (90))

We present some plots of the auto-correlation function $C(\tau+t_{\rm w2}+t_{\rm w1}, t_{\rm w2}+t_{\rm w1})$ in Figures 6 and 7 for the case of $d=1$. The generic feature is of course the same at any dimension but the dynamical exponent for the decay depends on the dimension as $\lambda = d/2$. Here the three-stage relaxation is clearly visible. Note that the plateau is visible only for the cases in which $t_{\rm w1} \gg t_{\rm w2}$, which is the condition to have sharp separation between the inner-coarsening and outer-coarsening.

Second, let us consider more complicated cases with non-zero $t_{\rm w3} > 0$. The reason we analyzed it is to make comparison with a set of conventional TRM data [7] where such a protocol is used[5]. Later in Section 6, we compare the result with an experimental data. In Figure 8 we show a plot of the auto-correlation function $C(\tau+t_{\rm w}^{\rm total}, t_{\rm w}^{\rm total})$ given in (110). We also show curves of the special case where $t_{\rm w1} \to \infty$. It can be seen that the initial decay does

[5] In any case, it may be impossible to realize strictly $t_{\rm w3}=0$ in experiments.

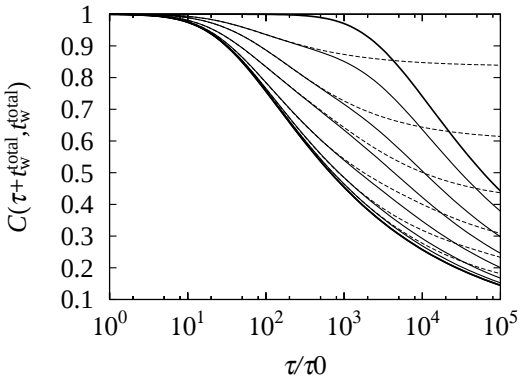

Fig. 8. The auto-correlation function $C(\tau + t_{\rm w}^{\rm total}, t_{\rm w}^{\rm total})$ with $t_{\rm w}^{\rm total} = t_{\rm w3} + t_{\rm w2} + t_{\rm w1}$ in the $O(n)$ Mattis model ($d = 1$) under one-step cycling plotted against the time difference τ in the third stage. In Section 6, we compare these curves with an experimental data of the relaxation of thermo-remanent magnetization after one-step temperature cycling. The thin solid lines are curves with common $t_{\rm w1} = 990$ and $t_{\rm w3} = 10$ but varying $t_{\rm w2} = 10^6, 10^5, 10^4, 10^3, 10^2, 10^1$ (from left to right). The dotted lines are the corresponding curves with $t_{\rm w1} = \infty$. The top and bottom bold solid lines are the reference curves of standard coarsening $C_0(\tau + 1000, 1000)$ and $C_0(\tau + 10, 10)$ respectively.

not depend on $t_{\rm w1}$ and decays as the case $t_{\rm w1} = \infty$. This is the inner-coarsening regime which then crossovers to the plateau regime. Finally, the departure from the plateau due to outer-coarsening becomes visible at around $L(\tau) \sim L(t_{\rm w3} + t_{\rm w1})$.

The plateau value is nothing but the staggered magnetization within the ghost domains at time $t_{\rm w3} + t_{\rm w2} + t_{\rm w1}$. The latter is naturally smaller for longer duration of the second stage $t_{\rm w2}$. But note that it also depends on $t_{\rm w3}$ because the staggered magnetization tends to go back to the full value 1 in the third stage (see (83)). The last feature imply that rejuvenation is obscured in this protocol. Nonetheless, for any $t_{\rm w2}$, the presence of rejuvenation (inner-coarsening regime) can be recognized by comparing with the curves with much larger $t_{\rm w1}$ as demonstrated in the figure.

4.6 Short time linear response functions in one-step cycling

Within the spherical Mattis model, it is also possible to study directly the linear response function exactly. We study it below for the one-step cycling protocol and focus especially on its behavior in the third stage. Here we will consider response functions $R(\Delta t + t, t)$ with fixed time separation Δt as a function of increasing time t. It is analogous to the relaxation of AC-susceptibilities $\chi''(\omega, t)$ of frequency $\omega = 1/\Delta t$ at time t. The advantage of studying $R(\Delta t + t, t)$ is that its analytical expression is simpler than that of $\chi''(\omega, t)$. Some details of the calculations are presented in Appendix C. We will find the anticipated crossover from inner-coarsening to outer-coarsening in the response sketched in Section 3.4.

It should be noted however that mean field theories [27–29] suggests long time behavior of the response is likely to be quite different between spin-glass and usual coarsening systems as we noted in Section 3.5. Nonetheless, as far as short-time response is concerned the generic behavior of the response function may be similar.

In the first stage the relaxation is the same as in the standard coarsening and we naturally find new relaxation also in the 2nd stage,

$$\begin{aligned} \tilde{R}_{\rm I}(\Delta t + t, t) &= \tilde{R}_0(\Delta t + t, t) \\ \tilde{R}_{\rm II}(\Delta t + t, t) &= \tilde{R}_0(\Delta t + (t - t_{\rm w1}), t - t_{\rm w1}). \end{aligned} \quad (114)$$

Here $\tilde{R}$ is the response function scaled by that in equilibrium and $\tilde{R}_0(\Delta t + t, t)$ is the rescaled response function of the standard coarsening (see Appendix C for the details).

One finds richer behavior of the short-time response in the 3rd stage $t_{\rm w3} + t_{\rm w2} + t_{\rm w1} > t > t_{\rm w2} + t_{\rm w1}$ as obtained in (C.11) and (C.12). We find the following. At the beginning of the third stage which is the inner-coarsening regime, we find new relaxation. On the other hand, in larger time scale which we called as plateau and outer-coarsening regime, we find continuation of the 1st stage.

$$\tilde{R}_{\rm III}(\Delta t + t, t) \simeq \tilde{R}_0(\Delta t + t - t_{\rm w2} - t_{\rm w1}, t - t_{\rm w2} - t_{\rm w1}) \quad \text{inner-coarsening regime} \quad (115)$$

$$\tilde{R}_{\rm III}(\Delta t + t, t) \simeq \tilde{R}_0(\Delta t + t - t_{\rm w1}, t - t_{\rm w1}) \quad \text{plateau/outer-coarsening regime} \quad (116)$$

In the case a) $L(t_{\rm w1}) \gg L(t_{\rm w2})$ which allows the plateau regime, the inner-coarsening regime finishes before the significant relaxation due to the outer-coarsening starts. The generic feature is consistent with the picture presented in Section 3.4 (see Fig. 4).

4.7 Multiplicative noise effect and 2-step U-turns in a 2-step cycling

One can extend the above calculations to two-step cycling $\alpha \to \beta \to \gamma \to \beta \to \alpha$, trying to mimic the multi-step cycling discussed in Section 3.6. Although the full calculation will be become too lengthy, we can readily have a glimpse of what happens in the spherical model.

Let us suppose that we are given a spin-configuration whose projection to a certain equilibrium state α is $\hat{\phi}_k^{\alpha}(0)$. We consider to give this as initial condition for a one-step cycling $\beta(t_{\rm w1}) \to \gamma(t_{\rm w2}) \to \beta(t_{\rm w3})$ and monitor the time evolution of the projection to α. One finds that the expectation value of the projection $\hat{\phi}_k^{\alpha}(t_{\rm w3} + t_{\rm w2} + t_{\rm w1})$ at

time $t_{\rm w3}+t_{\rm w2}+t_{\rm w1}$ as,

$$\langle\hat{\phi}_k^\alpha(t_{\rm w3}+t_{\rm w2}+t_{\rm w1})\rangle_\sigma = \int\frac{{\rm d}^dk_1}{(2\pi)^d}\int\frac{{\rm d}^dk_2}{(2\pi)^d}\int\frac{{\rm d}^dk_3}{(2\pi)^d}$$
$$\times\int\frac{{\rm d}^dk_4}{(2\pi)^d}\langle(\hat{\sigma}^{\alpha\beta})_{k_1}(\hat{\sigma}^{\beta\gamma})_{k_2}(\hat{\sigma}^{\gamma\beta})_{k_3}(\hat{\sigma}^{\beta\alpha})_{k_4}\rangle_\sigma$$
$$\times\frac{{\rm e}^{-(k-k_1)^2t_{\rm w3}}}{\sqrt{\Gamma_{1-{\rm step}}(t_{\rm w3}+t_{\rm w2}+t_{\rm w1},t_{\rm w1}+t_{\rm w2})}}\frac{{\rm e}^{-(k-k_1-k_2)^2t_{\rm w2}}}{\sqrt{G_0(t_{\rm w2},0)}}$$
$$\times\frac{{\rm e}^{-(k-k_1-k_2-k_3)^2t_{\rm w1}}}{\sqrt{G_0(t_{\rm w1},0)}}\hat{\phi}^\alpha_{k-k_1-k_2-k_3-k_4}(0)$$
$$= m_{\rm mem}(t_{\rm w3},t_{\rm w2},t_{\rm w1})C_0(t_{\rm w3}+t_{\rm w1},0)\hat{\phi}^\alpha_k(0). \qquad (117)$$

In the derivation of the last equation, we used (A.7), (59, 62) and (97). Thus we find that the expectation value of the projection field is proportional to the initial one $\hat{\phi}^\alpha_k(0)$ with time-dependent prefactor.

A remarkable point is that the prefactor is the product of $m_{\rm mem}(t_{\rm w3},t_{\rm w2},t_{\rm w1})$ and the auto-correlation function $C_0(t_{\rm w3}+t_{\rm w1},0)$. At the beginning of the last stage (2nd β-coarsening), we readily find that the prefactor is $C(t_{\rm w1},0)\rho$ where ρ is the reduction of the amplitude due to γ coarsening. The latter means a multiplicative reduction of the amplitude of the projection onto α due to the successive coarsening of two different phases (β and γ) as we conjectured in Section 3.6. The fact that noise effect is multiplicative, can be check explicitly in more general multi-step coarsening as presented in Appendix B (see (B.9)).

In the inner-coarsening regime of the last stage (2nd β-coarsening), we readily find that $m_{\rm mem}(t_{\rm w3},t_{\rm w2},t_{\rm w1})$ almost returns back to 1 within the recovery time $\tau_{\rm rec}$ so that the noise due to γ-coarsening onto β is now removed. As far as time separation is wide enough so that the plateau regime is allowed, the recovery time $\tau_{\rm rec}$ is much shorter than $t_{\rm w1}$. Within the plateau regime $C_0(t_{\rm w3}+t_{\rm w1},0)\simeq C_0(t_{\rm w1},0)$. Remarkably, then the above formula (117) implies that the noise onto α due to γ coarsening is also cured thanks to the 2nd β-coarsening and the remnant noise is now only that due to β phase. But if one perform the 2nd β-coarsening for too long, the factor $C_0(t_{\rm w3}+t_{\rm w1},0)$ will begin to decrease further meaning that the noise due to β coarsening will now affect the projection to α.

If one stops the 2nd β-coarsening at around $\tau_{\rm rec}$ and then switch to coarsening of α, the remnant noise due to β phase will be removed. The above result demonstrates that the system can be returned back to the starting point in the phase space by two-step U-turns. This is consistent with our picture presented in Section 3.6 for the recovery of memory in multi-step cycling.

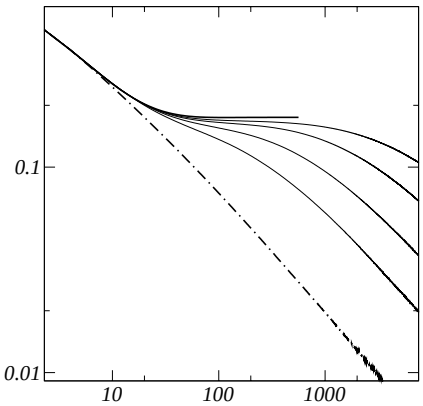

Fig. 9. The auto-correlation function $C(\tau+t_{\rm w2}+t_{\rm w1},t_{\rm w2}+t_{\rm w1})$ in the $d=2$ Ising Mattis model under one-step cycling plotted *versus* τ (MCS). The dotted lines are $t_{\rm w2}=20$ MCS and $t_{\rm w1}=100,300,1000,3000$ (MCS) from left to right. The solid line on the top is the case $t_{\rm w1}=\infty$. The dash-dotted line is the reference curve with zero-waiting time.

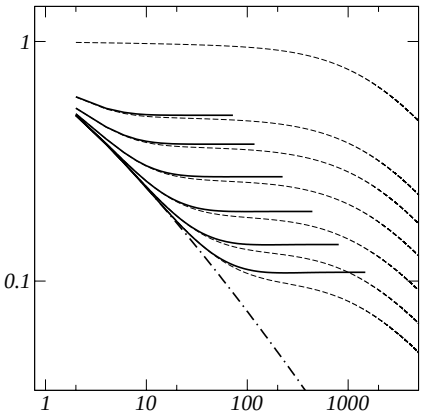

Fig. 10. The auto-correlation function $C(\tau+t_{\rm w2}+t_{\rm w1},t_{\rm w2}+t_{\rm w1})$ in the $d=2$ Ising Mattis model under one-step cycling plotted *versus* τ (MCS). The dotted lines are $t_{\rm w1}=1000$ MCS $t_{\rm w2}=0,2,4,8,16,30,50$ from the top to below. The solid lines are with $t_{\rm w1}=\infty$. The dash-dotted line is the reference curve with zero-waiting time.

5 Two-dimensional Ising Mattis model

While the $O(n)$ model in the spherical limit is analytically tractable and contains the essential phenomenology of coarsening systems, its drawback is that it does not contain topological defects like domain walls [52]. Thus it is desirable to study models which have clearly defined domain walls. In the present paper, we do not pursue more elaborate analytical calculations to take into account topological defects like the Ohta-Jasnow-Kawasaki approximation. Instead, we directly study the Mattis model introduced in Section 3.1 with Ising spins on a two-dimensional square lattice by Monte Carlo simulations.

The algorithm is zero temperature Monte Carlo dynamics with multi-spin coding. The spin configurations $\{\sigma_i^{\alpha(\beta)}\}$ in the ground states are chosen to take ±1 randomly.

5.1 Auto-correlation function after one-step cycling

We simulated the one step cycling process $A\to B\to A$ described in Section 3.3, which was studied in the $O(n)$

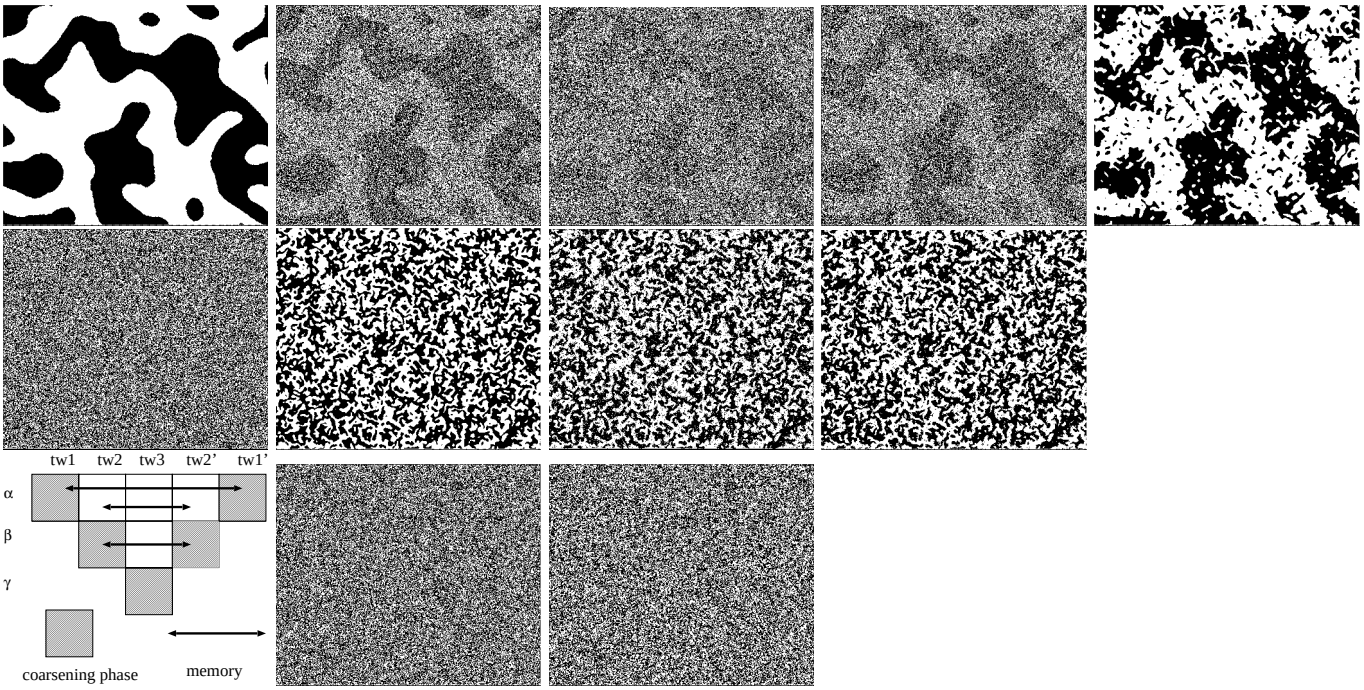

Fig. 11. The projection of the spin configuration onto the ground state A, B and C (from top to bottom) at the end of each stage in the in a 2-step cycling. The columns are in the chronological order. Here $t_{\rm w1} = 10000$, $t_{\rm w2} = 100$, $t_{\rm w3} = 2$, $t'_{\rm w2} = 4$, $t'_{\rm w1} = 200$ (MCS). The system size is 1024×1024.

model in Section 4.4. We examined the auto-correlation function between the configuration just at the beginning of the third stage and the temporal configuration after time τ in the third stage, which was studied in the $O(n)$ model in Section 4.5. The system size is 8192×8192 which is large enough to avoid finite size effects within the time window we have explored $\sim 10^4$ (MCS).

In Figures 9 and 10 we present the result of the auto-correlation function. We included the results of simulations in which the ground state of phase α is given to the second stage as the input, *i.e.* the $t_{\rm w1} = \infty$ limit. By comparing with the corresponding results within the spherical model shown in Figure 6 and 7, one can see a very similar structure of the relaxation curves in agreement with the conjecture presented in Section 3.5. The initial decay implies inner-coarsening regime where the correlation decays as if the memory of the first stage was completely lost. The subsequent behavior implies however that the memory of the first stage is not lost but its amplitude is reduced from 1 to $\rho < 1$ at the beginning of the third stage.

5.2 An example of multiple-memory

In Section 3.6 we discussed coarsening under cycling of multiple phases. Especially we argued that i) the noise effect of multiple phases is multiplicative and that ii) the multiplicative noises can be removed one by one by additional series of coarsening in the reversed order. We have verified the picture within the spherical model to a certain extent in Section 4.7. Here we present a demonstration of the coarsening under cycling of three independent target states in the 2-dimensional Ising Mattis model where the two features i) and ii) appear explicitly.

In Figure 11 we show the time evolution of the projection to three completely different ground states A, B and C during two-step coarsening $A(t_{\rm w1}) \to B(t_{\rm w2}) \to C(t_{\rm w3}) \to B(t'_{\rm w2}) \to A(t'_{\rm w1})$. We chose $t_{\rm w1} = 10\,000$, $t_{\rm w2} = 100$, $t_{\rm w3} = 2$, $t'_{\rm w2} = 4$ and $t'_{\rm w1} = 200$ (MCS). The time schedule is decided according to the principle explained in Section 3.6. First, the first series $A \to B \to C$ is designed such that the length scales of the three-phases are well-separated $t_{\rm w1} \gg t_{\rm w2} \gg t_{\rm w3}$. Second, the reversed series $B \to A$ is designed such that multiplicative noise is removed one by one without accumulating additional noise: $t_{\rm w2} > t'_{\rm w2} > t_{\rm w3}$ and $t_{\rm w1} > t'_{\rm w1} > t_{\rm w3}$.

One finds that the noise on A in the end of 3rd stage can be very large. This latter is due to the multiplicative effect of noise. It will take enormous time to remove the noise by a single stroke which well exceeds $t_{\rm w1}$ so that recovery of memory is hopeless. However, one can find that memory of the spin-configuration at the end of 2nd and 1st stages are recovered by the 4th and 5th stages respectively (as shown by arrows in the schematic diagram.) Thus this example demonstrates that multiple memories can be indeed stored and retrieved successively as argued in Section 3.3.

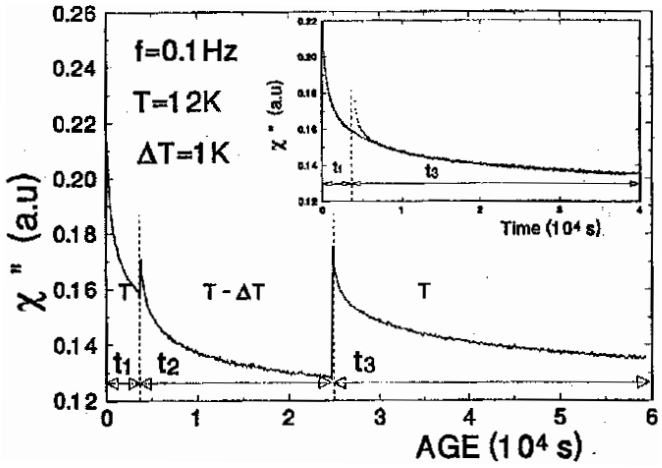

Fig. 12. Relaxation of χ'' during an one-step negative temperature-cycling experiment 12 K $\rightarrow$ 11 K $\rightarrow$ 12 K as a function of time. The inset shows points taken during the first and third stage at $T = 12$ K plotted against the total time spend at $T = 12$ K. The solid line is a reference relaxation curve of isothermal aging at $T = 12$ K.

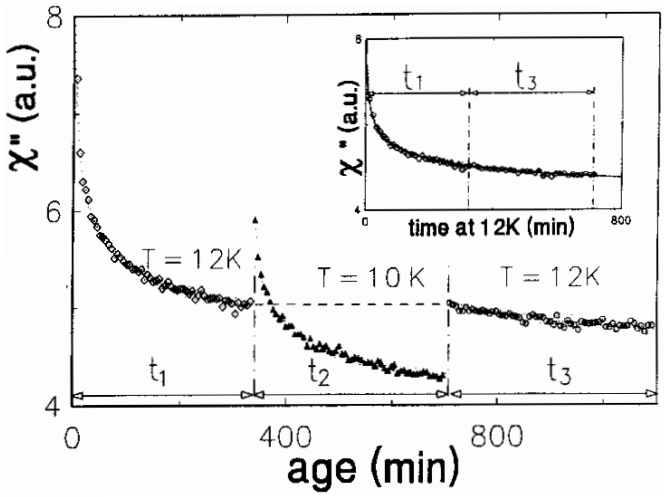

Fig. 13. χ'' relaxation during an one-step negative temperature-cycling experiment 12 K $\rightarrow$ 10 K $\rightarrow$ 12 K as a function of time. The inset shows points taken during the first and third stage at $T = 12$ K plotted against the total time spend at $T = 12$ K. The solid line is a reference relaxation curve of isothermal aging at $T = 12$ K.

6 Comparison with temperature-cycling experiments in spin-glasses

We now discuss the temperature-cycling experiments in spin-glass from the present point of view. For reference, we consider the data of experiments on the $CdCr_{1.7}In_{0.3}S_4$ ($T_c = 16.7$ K) insulating spin glasses. Because of the limitation of pages we cannot discuss another rich set of experimental results obtained in Cu:Mn metallic spin-glass [12–14] which show essentially the same features. For AC-susceptibility in one-step temperature cycling we refer to [10,11] and [15] for multi-step (continuous) temperature cycling. For DC-susceptibilities we refer to the measurements of thermo-remanent magnetization (TRM) on the same $CdCr_{1.7}In_{0.3}S_4$ system reported in [7] which can also be found in [8].

6.1 AC-susceptibility in one step temperature-cycling experiments

We consider first the measurements of the out-of-phase AC susceptibility $\chi''(\omega, t)$ in a one-step temperature cycling procedure, and interpret them according to the picture presented in Section 3.3 and Section 3.4. In Figure 12 the data [10] of the relaxation of $\chi''(\omega, t)$ at $\omega/2\pi = 0.1$ Hz is shown. Note that the schematic picture presented in Figure 4 agrees well with the general feature of the data. The third regime can be naturally understood as containing both the inner-coarsening regime and outer-coarsening regime in a well separated manner. We expect that the duration of the inner-coarsening regime is given by (21). This yields $\tau_{\rm rec} \simeq 700$ (sec) at 12 K using the microscopic time scale $\tau_0 = 10^{-13}$ (sec) and the duration of the second stage $t_{\rm w2} \sim 2 \times 10^4$ (sec) at 11 K. The order of magnitude of the latter is compatible with the duration of the transient relaxation ~ 2500 (sec) seen at the beginning of the third stage.

In Figure 13 the data [11] of a similar experiment but with a larger ΔT is shown. In this case the relaxation of the inner-coarsening regime is expected to be, from (21), $\tau_{\rm rec} \simeq 27$ (sec) using $\tau_0 = 10^{-13}$ (sec) and the duration of the second stage $t_{\rm w2} \sim 350$ (min). Note that this is of the same order of the period of the AC measurement $2\pi/\omega \sim 10$ (sec) so that condition (24) needed to observe the inner-coarsening regime is barely satisfied. Because of the temperature dependence of the stiffness of the barrier (8), $\tau_{\rm rec}$ would be even shorter and the condition (24) would be strongly violated. This could explain why the transient relaxation seen in Figure 12 is absent from the data, and that full memory can be expected.

Now let us consider the data [10] corresponding to a positive cycling in the same system, which is shown in Figure 14. In this case the duration of the second stage $t_{\rm w2} \sim 6000$ (sec) at 13 K amounts to effective time (5) of 10^5 sec at 12 K, which is much larger than the duration of the first stage ($t_{\rm w1} \sim 4000$ (sec)). Thus in the third regime we expect that the inner-coarsening regime and outer-coarsening are not separated, and that the obtained relaxation is very close to the one obtained in the first regime (no memory).

To summarize we found that the present picture is compatible with the experimental data of the out-of-phase AC susceptibility during one-step temperature cycling. In particular, the memory effect for negative cycling is explained by the fact that the inner-coarsening regime ends after a time so short that it cannot be observed.

In the cases discussed above, we did not need to take into account the fact that the overlap length $\xi_{\Delta T}$ become very large when $\Delta T \rightarrow 0$. However it should be noted that the overlap length associated with any fluctuations of

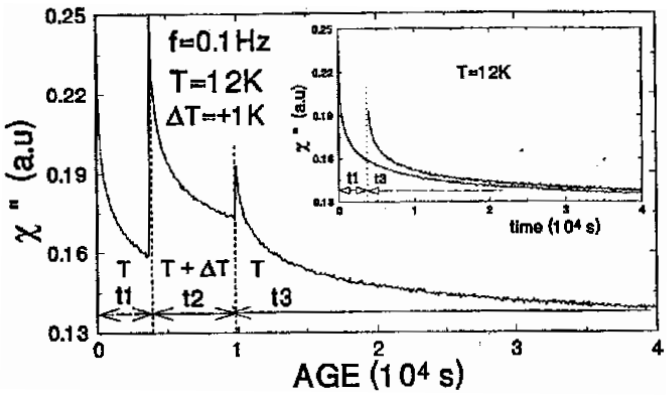

Fig. 14. χ'' relaxation during an one-step positive temperature-cycling experiment 12 K $\rightarrow$ 13 K $\rightarrow$ 12 K as a function of time. The inset shows points taken during the first and third stage at $T = 12$ K plotted against the total time spend at $T = 12$ K. Note that the second curve can nearly be superimposed onto the first one by an horizontal shift of 4000 seconds.

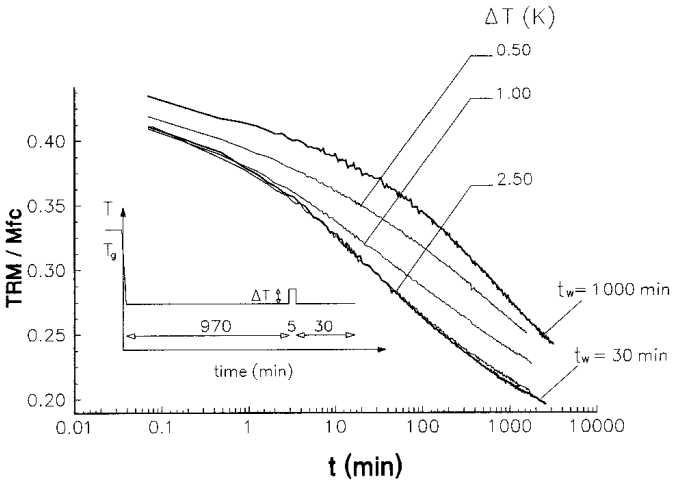

Fig. 15. Relaxation of the thermo-remanent magnetization (TRM) at 12 K after a one-step positive temperature-cycling. The procedure is shown in the inset. The reference curves of $t_{\rm w} = 30$ (min) and $t_{\rm w} = 1000$ (min) of standard (isothermal) aging are also shown.

temperatures in experiments should be large enough compared with the dynamical length scales explored. Otherwise experimental temperature becomes meaningless. Indeed, there are some data which suggest that $\xi_{\Delta T}$ depends on ΔT [13]. For example the data of negative cycling between very close temperatures 12 $\rightarrow$ 11.7 K $\rightarrow$ 12 K of the insulating spin-glass shown in [11] reveals that the relaxation during the second stage at 11.7 K 'helps' relaxation at 12 K to a certain extent.

6.2 DC-susceptibility in one step temperature-cycling experiments

Let us now consider the relaxation of the thermo-remanent magnetization (TRM), which is a DC susceptibility, after similar one-step cycling. A representative data set is shown in Figure 15 which is taken from [8]. Here a positive temperature cycling 12 K $\rightarrow$ 12 K + ΔT $\rightarrow$ 12 K is done under small magnetic field which is then cut-off. Then the subsequent relaxation of the magnetization is measured. Here the duration of the second stage is fixed to 5 minutes but the amplitude of the shift ΔT is varied.

Now let us compare the experimental data with the correlation function after a one-step cycling in the $O(n)$ Mattis model, which we analyzed in Section 4.5. Here we suppose that the generic features of the correlation function and TRM decay are similar. It should however be noted that this is not obvious since the violation of the fluctuation dissipation theorem (FDT) in such non-stationary situations [27,29,30] does not allow an exact identification of the two quantities. Second, we again disregard the possible finite value of $\xi_{\Delta T}$ between the different equilibrium states at different temperatures and consider that they are completely uncorrelated.

The activated dynamics (3) implies that for larger ΔT, the coarsening in the second stage reaches larger length scales $L_{12\ {\rm K}+\Delta T}(t_{\rm w2})$, so that more 'noise' is added to the 12 K domain structure. Thus we suppose that larger ΔT in the experiment corresponds to larger $t_{\rm w2}$ in our model. Indeed the experimental curves shown in Figure 15 appear to be very similar to the result in the $O(n)$ Mattis model shown in Figure 8.

In Section 4.5, we found that the generic features of the auto-correlation function can be understood as crossover from rejuvenation (inner coarsening) to memory (outer-coarsening). This crossover is sharp only in the case a) where the second stage is effectively much shorter than the first stage ($t_{\rm w2} \ll t_{\rm w1}$). On the other hand, in the case b) where the second stage is effectively much longer than the first stage, rejuvenation is nearly complete.

Let us note that the curve in Figure 8 with $\Delta T = 2.5$ K belongs to the case b) because the effective time (5) of 5 minutes at 14.5 K amounts to 8400 min at 12 K (with $\tau_0 \sim 10^{-13}$ (sec)), which is very large compared with $t_{\rm w1} = 970$ min. On the other hand, $\Delta T = 1.5$ K and 1 K can be considered as cases of a) since their effective time 430 min and 97 min at 12 K are smaller than $t_{\rm w1}$. It would be very interesting to look experimentally for the plateau regime as seen in Figures 6, 7, 8 and Figures 9, 10.

6.3 Multiple step temperature-cycling

Finally let us consider the multiple-step (continuous) version of the temperature cycling which has been studied in recent experiments [12,14–16] using the out-of-phase AC susceptibility $\chi''(\omega, t)$. Here we discuss based on the scenario we developed in Section 3.6. In Figure 16 an example of the data taken from [15] is shown.

The basic schedule is a negative-cycling which consist of cooling and heating procedure. In the cooling, the temperature is reduced successively by 'micro-quenches' of small temperature step ΔT, $T_i = T_{\rm start} - {\rm i}\Delta T$ with $(i = 1, 2, \ldots, n)$ where $T_{\rm start}$ is the starting temperature

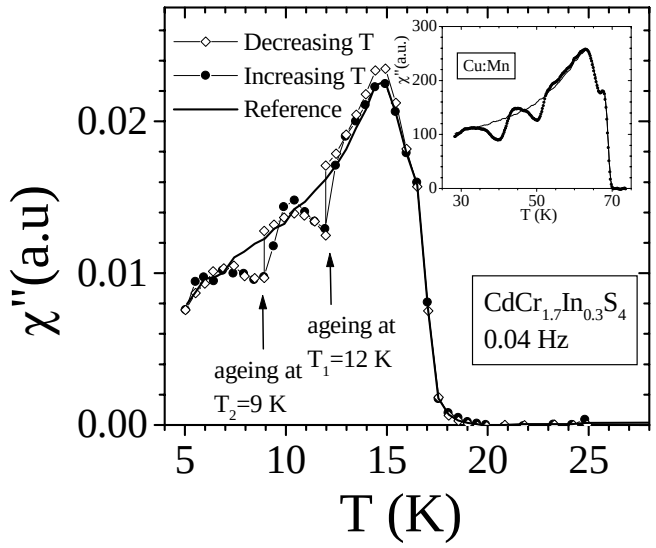

Fig. 16. Out-of-phase susceptibility χ'' of the $CdCr_{1.7}In_{0.3}S_4$ spin glass. The solid line is measured upon heating the sample at a constant rate of 0.1 K/min (reference curve). The data during cooling (not shown) lies close to but slightly above the solid line. Open diamonds: the measurement is done during cooling at this same rate, except that the cooling procedure has been stopped at 12 K during 7 h and then 40 h at 9 K to allow for aging. Cooling then resumes down to 5 K: χ'' is not influenced and goes back to the reference curve (rejuvenation, from Ref. [15]). Full circles: after this cooling procedure, the data is taken while re-heating at the previous constant rate, exhibiting memory of the aging stage both at 9 K and 12 K. The inset shows a similar "double memory" experiment performed on the Cu:Mn metallic spin glass.

and n is the number of steps. At every temperature T_i a short period of time $t_i = \Delta t$ is spent. In this experiment, $\Delta T = 0.5$ K and $\Delta t = 5$ min [34]. In the heating. the temperature is raised back successively by the same ΔT with a the same period $t'_i = \Delta t$ at each temperature.

Within the present scenario, coarsening of new phases are expected at every temperature in the cooling and the heating is the reversed order series of coarsening. Note that the above basic schedule satisfies the condition (33) to retrieve the memory at each temperature in the heating. For instance (21) implies the noise due to $\Delta T = 5$ min at 10 K on the phase at $10 + \Delta T = 10.5$ K can be erased quickly within $\tau_{\rm rec} \sim 1$ (min). Indeed, it is found in the experiment that the reference curve of cooling and heating lie close to each other [15]. Concerning the frequency of AC $\omega/2\pi \sim 0.04$ (Hz), we need to suppose that it is low enough so that the signal of the cleaning (inner-coarsening) does not blur the observation of the memory.

In the experiment, an interesting modification is made for the cooling procedure: now two special temperatures (9 and 12 K) are chosen to make relatively long stops $t_{\rm stop} \sim 40,7$ hours in stead of the short period $\Delta t = 5$ min. But all the rest of the basic schedule is unchanged. The dips in cooling curve mean relaxation due to the long aging. Then the fact that the cooling curve tend to return to the reference curve (without stops) after the long stops implies coarsening of the new phase within the present scenario.

Let us the consider the heating curve. As the temperature comes up to the stop temperature 9 K, the curve goes downward tracing the cooling curve. The latter is expected within the present scenario since as soon as the noise due to coarsening at lower temperatures are erased, we are left with the large ghost domain at 9 K with its full amplitude recovered. The same phenomena happens also for 12 K.

The phases at the temperatures just above 9 K and 12 K are expected to be very noisy due to the long stops. The latter belongs to the case b) discussed in Section 3.3.2 and their memory may be hardly retrieved. Then the increase of the heating curve after passing the stop temperatures may be interpreted as the signal of inner-coarsening (rejuvenation). Furthermore, the long stop at 9 K of 40 hours could have affected the memory at 12 K. However, its effective time turns out to be only 4 sec at 12 K. If the stop temperatures are closer, the recovery of memory could have been affected more. Such a phenomena is indeed observed in some experiments [16].

Finally let us also note that the 'dips' are rounded in the experimental data, while we would have expected sharper dips. In the present scenario, the rounding of the dips may be attributed to finiteness of the overlap length.

7 Summary and open problems

7.1 What we have done in this paper

The basis of our approach in the present study is the droplet picture. The fundamental ingredients of the present paper are the tenets of the droplet theory, namely: i) for a given temperature below the critical temperature, there are only two equilibrium states related by a global flip; ii) the relaxational dynamics is the coarsening of the domains of these equilibrium states. The growth of the domains is due to the thermal activation of droplets; iii) the underlying equilibrium states change chaotically with weak external perturbations, such as a change of temperature.

By a combination of scaling arguments, analytical calculations and numerical simulations, we have demonstrated the *preservation and retrieval of memory* is possible in a purely dynamical way in the absence of any underlying static backbone structure. First, we showed that *preservation of memory* is possible by 'ghost domains' (domain wall structure plus noise) of *all* the phases the system goes through in the temporal spin-configuration. Here coexistence of statistically independent domains only amount to mutual injection of uncorrelated short-range noise which do not destroy the large scale spatial structures of each other. Thus in order to describe the spin-configuration, one needs to keep track of the projections to all phases. In this sense, there are indeed many 'phases' in the temporal spin-configuration, as already anticipated

in the experimental studies [7,8]. Then we studied in detail *retrieval of memory*: how the noise on a phase due to coexistence of the domain structures of other phases can be removed by additional conjugate coarsening. The analysis has been carried out explicitly in term of various spatial/temporal correlation functions and linear response functions. In particular, we have shown that when the time spent in the intermediate state is sufficiently small, rejuvenation effects and memory effects can be observed in a well separated manner. Therefore the difficulty of the previous works [5,6,13] to explain the 'memory effect', is resolved. It is rather surprising to find that the simplest version of the droplet picture already contains a consistent and rather rich phenomenology which can account for experiments at least qualitatively.

7.2 Is the picture totally satisfactory?

The droplet picture itself is based on phenomenological scaling arguments and Migdal-Kadanoff type real-space renormalization-group calculations [1,2]. It is by no means obvious that real spin-glasses can be described within this simple scenario. Many papers have appeared recently, presenting relatively strong evidence against the simplest version of the droplet theory [39,41,42]. On the other hand evidence for the validity of the basic droplet picture has also been provided [43–45,80–82]. In the present paper we have focused on the simplest version of the droplet theory. Any modifications due to possible corrections to the simplest version go beyond the scope of the present paper and we leave this issue for future studies.

The theoretical situation of temperature chaos is also far from being settle neither in low dimensional systems nor in mean-field models. Early numerical investigations at finite temperatures [70,71] suggests chaos with magnetic field and with the change of couplings. Temperature chaos has been found in 2-d Edwards-Anderson model [73] for very large length scales. Temperature chaos has also been suggested by some analytical studies of mean-field models [35,36,38]. However recent simulations of both the SK and the 3d Edwards-Anderson models have concluded on the absence of chaos with temperature [72] (as also suggested by another analytical calculation for the SK model [37]). But there is still a possibility that temperature-chaos was not observed in the latter because the overlap length is larger than the system sizes studied. Chaotic changes of equilibrium states have also been looked for other related glassy systems. For instance, a large scale transfer-matrix study of an elastic string pinned in random media [3], which describes for instance pinned domain walls, has found some evidence for the chaotic change of the free-energy landscape with temperature again for very large length scales. All studies therefore suggest that 'chaos', if it exists, only occurs on large length scales, whereas the dynamical length is expected to be modest, even in experimental studies [77,78], due to its very slow growth with time.

7.3 An alternative picture

Let us now briefly compare the present scenario based on the droplet picture with another phenomenology [7,8], based on a dynamical interpretation of the Parisi solution of the SK (mean-field) model, which suggests that the energy landscape is hierarchical. A concrete implementation of this picture was proposed in [24], in terms of a thermally activated generalized random-energy model (GREM). To each level of the hierarchical tree is associated a transition temperature, such that the dynamics at this level is stationary for higher temperatures, and aging for smaller temperatures. A small decrease of temperature induces some rejuvenation by driving out of equilibrium a new level of the tree, while freezing out the dynamics at the upper levels, thereby allowing the memory to be conserved. This model was recently studied further in [26], where it is shown numerically that the rejuvenation/memory effect is indeed already reproduced with two levels.

A real space interpretation of this hierarchical tree proposed in [24,60], and further developed in [23], in terms of a multi-scale dynamics. Low levels of the tree corresponds to short wavelength modes, which are only frozen at low temperature, while large wavelengths modes are frozen at a higher temperature and constitute the 'backbone' where the memory is imprinted. The picture is particularly clear in the context of pinned domains walls [23], and should apply to disordered ferromagnets where the slow dynamics comes from the motion of these pinned domain walls [19,21].

A closer look at the two different scenarios shows that they actually share several important points. The fact that the dynamics is thermally activated is crucial in both pictures, as it provides a natural separation of time scales for different length scales and/or temperatures. As was pointed out in [23], for a given experimental time window, temperature acts as a microscope by selecting the relevant dynamical length scales. The way memory is conserved is therefore common in both approaches: it is stored in large length scales which are to a large extent unaffected by the small length scale dynamics taking place at lower temperatures. However it should be noted that in the droplet picture, there is no *static* backbone structure in the phase space and the memory is entirely a dynamical effect. The mechanism leading to rejuvenation is therefore different in the two pictures: in the droplet picture, it is due to a complete modification of the free energy landscape with temperature, whereas in the hierarchical picture it is due to the progressive freezing of smaller and smaller wavelengths [23]. This picture is consistent with the simulations of [72]: a broad peak in the overlap probability at high temperature is resolved into sharper and sharper subpeaks as the temperature is lowered, with no overall shift.

One should finally note that comparable rejuvenation/memory effects have now been seen in very different materials, such as PMMA [17], where the droplet model is probably not the appropriate picture. In this respect, the idea of progressive freezing of smaller and smaller length scales is perhaps more generic.

7.4 Further developments

In the present paper, we discussed experimental data only qualitatively. More detailed and critical examinations of the scenario developed in the present paper should be done. It would be very interesting to look for the plateau regime which separates the rejuvenation and memory both in experiments and numerical simulations.

A crucial difference between the two pictures is therefore the existence of an overlap length $\xi_{\Delta T}$ in the droplet picture. The role of this length (that we have neglected in the present paper to focus on the phenomena on larger time scales) should show up when the temperature change is very small (or equivalently shorter time scales are considered), and therefore be important to account for the possible cooling rate effects [9,15] in spin-glasses. We hope to come back to this important point in the future. We have furthermore neglected the fact that the energy barriers are expected to be temperature dependent in the droplet picture through the temperature dependence of the stiffness (8). This leads to a super-activated behavior of the time scales, as was seen in [50], that needs to be quantitatively accounted for [51,82].

If chaotic change of equilibrium states can be made by non-thermal perturbations like change of magnetic field [70] or pressure, they will also provide useful means to examine the present scenario. Temperature changes may be used simultaneously to enhance the time separations. If the present picture is correct, such a non-thermal perturbation at $T-\Delta T$ should induce the growth of domains on very short length scales, an effect that can be erased quickly by heating up the system. Therefore, complete memory should also be observed in a protocol where: $T \to T - \Delta T \to T$ and the strength of the strength of non-thermal perturbation P is changed as $P = 0 \to P = \Delta P \to P = 0$ simultaneously.

Another good testing ground for the two approaches may be systems with pinned-domain walls which is intimately related with the problem of elastic manifolds in random media [57–61,3,62] whose dynamics show aging effects [28,29,63–67]. As we noted above a very natural scenario can be obtained by a GREM based approach [23]. On the other hand, it is also straightforward to construct a scenario based on a droplet picture [3] for this problem in a way similar to our present work. A suitable toy model corresponding to the spherical Mattis model we studied here is the elastic manifold pinned by quenched random force field (Larkin model) subjected to cycling of the realization of the random force field. Concerning this issue, it is interesting to note that recent experiments on disordered ferromagnets and ferro-electrics have revealed several similarities with spin-glasses [19,21].

7.5 Some remarks on numerical simulations

A discouraging point of the numerical approach is that the separation of time scales cannot be made so dramatic like in experiments on spin-glasses. However, possible differences between experiments and simulations due to such a difference of time scales should be amenable to a quantitative analysis. One of the great advantages of the numerical approach is that one can directly obtain the size of the domains $L_T(t)$ at each time step using a spatial correlation functions between two real replicas [79]. Then the scaling ansatz presented in the present paper can be tested very precisely since everything can be expressed in terms of the size of the domains $L_T(t)$. Indeed this approach has been very useful to test some scaling ansatz by the droplet picture [5] for isothermal aging [80,82]. Furthermore, combined with an analysis on equilibrium properties around and below the critical temperature [81], this kind of approach allows one to quantitatively analyze possible crossovers between critical and low-temperature behaviors in the dynamical observables and in the domain growth law itself [82].

It is important to note that due to thermally activated processes which presumably dominate relaxational dynamics in spin-glass like systems, the *length scales* explored in simulations are actually very small. This might be the reason why rejuvenation/memory effects are hard to observe numerically [46–48], because both the above scenarios rely on the existence of non overlapping (in length scales) dynamical processes.

The fact that the growth law is so slow also implies that both experiments and simulations will never be in the *ideal* regime of asymptotically large length scales to test the scaling predictions of droplet picture. Whether one can observe some clear signatures of the droplet picture within a realistic time scale may then depend very much on details of the systems studied in experiments and simulations. Whether the usual Edwards-Anderson model is the best model to describe real spin-glass systems is now hotly discussed [49,48].

We want to thank E. Vincent for the permission to use the curves of the series of experiments in Saclay, useful discussions and encouragement. We want to thank S. Miyashita, M. Hammann, H. Chaté, S. Franz, F. Ricci, P. Nordblad, P. Jonason and R. Matthieu for useful discussions. H.Y. want to thank H. Takayama, K. Hukushima, T. Komori and L. Bernardi for useful discussions in the collaborations with them which have motivated the present work.

Appendix A: Properties of the transformation field

Here we summarize some useful statistical properties of the transformation field introduced in (42). Due to (41), the Fourier components of projection to different equilibrium states, say α and β, are related as,

$$\hat{\phi}^{\alpha}_{k} = \int \frac{\mathrm{d}^d k'}{(2\pi)^d} (\hat{\sigma}^{\alpha\beta})_{k'} \hat{\phi}^{\beta}_{k-k'}, \tag{A.1}$$

where we defined

$$(\hat{\sigma}^{\alpha\beta})_k = \int \mathrm{d}^d x \sigma^{\alpha\beta}(x) \mathrm{e}^{\mathrm{i}kx}. \tag{A.2}$$

The average becomes zero due to (43),

$$\langle(\hat{\sigma}^{\alpha\beta})_k\rangle_\sigma = 0. \tag{A.3}$$

and the 2-body correlation function is obtained using (44) as,

$$\langle(\hat{\sigma}^{\alpha\beta})_k(\hat{\sigma}^{\alpha\beta})_l\rangle_\sigma = \int \mathrm{d}^d x \mathrm{d}^d x' \langle\sigma_x^{\alpha\beta}\sigma_{x'}^{\alpha\beta}\rangle_\sigma \mathrm{e}^{\mathrm{i}kx}\mathrm{e}^{\mathrm{i}kx'} = \Delta(2\pi)^d\delta^d(k+l). \tag{A.4}$$

The 4-body correlation function in the real space is,

$$\begin{aligned}\langle\sigma^{\alpha\beta}(x_1)\sigma^{\alpha\beta}(x_2)\sigma^{\alpha\beta}(x_3)\sigma^{\alpha\beta}(x_4)\rangle_\sigma = \\ \Delta^2\{\delta^d(x_1-x_2)\delta^d(x_3-x_4)+\delta^d(x_1-x_3)\delta^d(x_2-x_4) \\ +\delta^d(x_1-x_4)\delta^d(x_2-x_3)\} \\ -2\Delta^3\delta^d(x_1-x_2)\delta^d(x_2-x_3)\delta^d(x_3-x_4),\end{aligned} \tag{A.5}$$

which becomes in the Fourier space,

$$\begin{aligned}\langle(\hat{\sigma}^{\alpha\beta})_{k_1}(\hat{\sigma}^{\alpha\beta})_{k_2}(\hat{\sigma}^{\alpha\beta})_{k_3}(\hat{\sigma}^{\alpha\beta})_{k_4}\rangle_\sigma = \\ \Delta^2\{(2\pi)^d\delta^d(k_1+k_2)(2\pi)^d\delta^d(k_3+k_4) \\ +(2\pi)^d\delta^d(k_1+k_3)(2\pi)^d\delta^d(k_2+k_4) \\ +(2\pi)^d\delta^d(k_1+k_4)(2\pi)^d\delta^d(k_2+k_3)\} \\ -2\Delta^3(2\pi)^d\delta^d(k_1+k_2+k_3+k_4).\end{aligned}$$

We will also need to consider projections to three different states say α, β and γ. A useful correlation function is,

$$\begin{aligned}\langle\sigma^{\alpha\beta}(x_1)\sigma^{\beta\gamma}(x_2)\sigma^{\gamma\beta}(x_3)\sigma^{\beta\alpha}(x_4)\rangle_\sigma = \\ \Delta^2\delta^d(x_1-x_4)\delta^d(x_2-x_3),\end{aligned} \tag{A.6}$$

which becomes in the Forier space,

$$\begin{aligned}\langle(\hat{\sigma}^{\alpha\beta})_{k_1}(\hat{\sigma}^{\beta\gamma})_{k_2}(\hat{\sigma}^{\gamma\beta})_{k_3}(\hat{\sigma}^{\beta\alpha})_{k_4}\rangle_\sigma = \\ \Delta^2(2\pi)^d\delta^d(k_1+k_2)\times(2\pi)^d\delta^d(k_3+k_4)\end{aligned} \tag{A.7}$$

Finally, correlation of the generalized type (45) becomes in the Fourier space,

$$\begin{aligned}\langle\hat{\sigma}_{k_1}^{\alpha_1\alpha_2}\hat{\sigma}_{k_2}^{\alpha_2\alpha_3}\ldots\hat{\sigma}_{k_{n-1}}^{\alpha_{n-1}\alpha_n}\hat{\sigma}_{k_n}^{\alpha_n\alpha_1}\rangle_\sigma \\ = (\Delta(2\pi)^d)^n\delta^d(k_1+k_2+\ldots+k_n).\end{aligned} \tag{A.8}$$

Appendix B: Properties of noise induced by coarsening of unrelated phase

Here we consider a projection field $\phi^\alpha(x)$ associated with a ground state $\sigma^\alpha(x)$ and study the effect of coarsening with respect to an unrelated ground state $\sigma^\beta(x)$.

We assume that the initial projection field $\phi^\alpha(x,t')$ satisfies the normalization condition $(\phi^\alpha(x,t'))^2 = 1$ at any x which implies,

$$\hat{\phi}_k^\alpha(t')\hat{\phi}_l^\alpha(t') = (2\pi)^{2d}\delta^d(k+l)W_k^\alpha(t'), \tag{B.1}$$

where

$$\int \mathrm{d}^d k W_k^\alpha(t') = 1. \tag{B.2}$$

due to (49) and (50). Given a spin configuration whose projection to a ground state $\sigma^\alpha(x)$ is $\phi^\alpha(x,t')$ at time t', we project it to the ground state $\sigma^\beta(x)$ to prepare the initial configuration. Using (A.1), the initial condition can be read as,

$$\hat{\phi}_k^\beta(t') = \int \frac{\mathrm{d}^d k'}{(2\pi)^d}(\hat{\sigma}^{\alpha\beta})_{k'}\hat{\phi}_{k-k'}^\alpha(t'). \tag{B.3}$$

Because of the random mapping through the transformation field $(\hat{\sigma}^{\alpha\beta})_k$, the resultant $\hat{\phi}_k^\beta(t')$ should also be a random field. Using (A.3), we find that the mean is zero,

$$\langle\hat{\phi}_k^\beta(t')\rangle_\sigma = \int \frac{\mathrm{d}^d k'}{(2\pi)^d}\langle(\hat{\sigma}^{\alpha\beta})_{k'}\rangle_\sigma\hat{\phi}_{k-k'}^\alpha(t') = 0. \tag{B.4}$$

Using (A.4), the correlation function becomes,

$$\begin{aligned}\langle\hat{\phi}_k^\beta(t')\hat{\phi}_l^\beta(t')\rangle_\sigma = \\ \int\frac{\mathrm{d}^d k'}{(2\pi)^d}\int\frac{\mathrm{d}^d l'}{(2\pi)^d}\langle(\hat{\sigma}^{\alpha\beta})_{k'}(\hat{\sigma}^{\alpha\beta})_{l'}\rangle_\sigma\phi_{k-k'}^\alpha\phi_{l-l'}^\alpha \\ = \Delta(2\pi)^d\delta^d(k+l).\end{aligned} \tag{B.5}$$

In the last equation, we used (B.1) and (B.2). To summarize, the initial condition for the coarsening is a random initial condition which has only short-range correlation. The solution of the equation of motion with such random initial condition is known and shown in (59).

By transforming the solution of $\hat{\phi}_k^\beta(t)$ at time $t(>t')$ back to the ground state σ^α through (A.1), we obtain the projection field as,

$$\begin{aligned}\hat{\phi}_k^\alpha(t) &= \int\frac{\mathrm{d}^d k'}{(2\pi)^d}(\hat{\sigma}^{\alpha\beta})_{k'}\hat{\phi}_{k-k'}^\beta(t) \\ &= \int\frac{\mathrm{d}^d k'}{(2\pi)^d}(\hat{\sigma}^{\alpha\beta})_{k'}\frac{\mathrm{e}^{-(k-k')^2(t-t')}}{\sqrt{\Gamma_0(t,t')}}\hat{\phi}_{k'}^\beta(t') \\ &= \int\frac{\mathrm{d}^d k'}{(2\pi)^d}(\hat{\sigma}^{\alpha\beta})_{k'}\frac{\mathrm{e}^{-(k-k')^2(t-t')}}{\sqrt{\Gamma_0(t,t')}} \\ &\quad\times\int\frac{\mathrm{d}^d k''}{(2\pi)^d}(\hat{\sigma}^{\alpha\beta})_{k''}\hat{\phi}_{k-k'-k''}^\alpha(t').\end{aligned} \tag{B.6}$$

In the following we examine the statistical property of the resultant projection field.

Using (A.4, 59) and (62) we obtain the expectation value of the resultant projection field as,

$$\begin{aligned}\langle\hat{\phi}_k^\alpha(t)\rangle_\sigma &= \int\frac{\mathrm{d}^d k'}{(2\pi)^d}\int\frac{\mathrm{d}^d k''}{(2\pi)^d}\langle(\hat{\sigma}^{\alpha\beta})_{k'}(\hat{\sigma}^{\alpha\beta})_{k''}\rangle_\sigma \\ &\quad\times\frac{\mathrm{e}^{-(k-k')^2t}}{\sqrt{\Gamma_0(t,t')}}\hat{\phi}_{k-k'-k''}^\alpha(t') \\ &= \frac{\Delta}{(2\pi)^d}\int\mathrm{d}^d k'\frac{\mathrm{e}^{-(k-k')^2t}}{\sqrt{\Gamma_0(t,t')}}\hat{\phi}_k^\alpha(t') \\ &= C_0(t-t',0)\hat{\phi}_k^\alpha(t').\end{aligned} \tag{B.7}$$

By taking inverse Fourier transform we obtain,

$$\langle\phi^\alpha(x,t)\rangle_\sigma = C_0(t-t',0)\phi^\alpha(x,t')\cdot \tag{B.8}$$

We find that the profile of the field is maintained on average with a reduced amplitude even after coarsening with respect to completely unrelated phase. The amplitude decreases as the system de-correlates from the initial configuration by coarsening. We have discussed a special case with an initial condition in which symmetry is fully-broken and found that the symmetry remains broken at any time. The above result is the solution with general initial conditions.

One can consider more general case where coarsening of multiple different equilibrium states are performed successively. Suppose that coarsening of n different equilibrium states, which are unrelated with α and with each other, are performed in succession between (t_{n-1},t'), (t_{n-2},t_{n-1}), $\ldots$, (t_1,t_2) and (t,t_1). Then following similar calculation and using (A.8) the projection field of α is obtained as,

$$\langle\phi^\alpha(x,t)\rangle_\sigma = C_0(t-t_1,0)C_0(t_1-t_2,0)\ldots C_0(t_{n-1}-t',0)\phi^\alpha(x,t'). \tag{B.9}$$

We find that the profile of the field is maintained with the amplitude reduced multiplicatively every time when a new unrelated phase is coarsened on top of it.

Next we consider the spatial correlation function of the resultant projection field. Using (A.6), (59), (62), (B.1) and (B.2) we obtain,

$$\begin{aligned}\langle\hat\phi^\alpha_k(t)\hat\phi^\alpha_l(t)\rangle_\sigma &= \int\frac{\mathrm{d}^dk'}{(2\pi)^d}\int\frac{\mathrm{d}^dk''}{(2\pi)^d}\int\frac{\mathrm{d}^dl'}{(2\pi)^d}\\ &\times\int\frac{\mathrm{d}^dl''}{(2\pi)^d}\langle(\hat\sigma^{\alpha\beta})_{k'}(\hat\sigma^{\alpha\beta})_{k''}(\hat\sigma^{\alpha\beta})_{l'}(\hat\sigma^{\alpha\beta})_{l''}\rangle_\sigma\\ &\times\frac{\mathrm{e}^{-(k-k')^2(t-t')}}{\sqrt{\varGamma_0(t,t')}}\frac{\mathrm{e}^{-(l-l')^2(t-t')}}{\sqrt{\varGamma_0(t,t')}}\hat\phi^\alpha_{k-k'-k''}(t')\hat\phi^\alpha_{l-l'-l''}(t')\\ &= C_0^2(t-t',0)\hat\phi^\alpha_k(t')\hat\phi^\alpha_l(t')\\ &+\varDelta(2\pi)^d\delta^d(k+l)\Big[1-2C_0^2(t-t',0)\\ &+\frac{1}{\varGamma_0(t-t',0)}\frac{\varDelta}{(2\pi)^d}\int\mathrm{d}^dk'\\ &\times\int\mathrm{d}^dl'\mathrm{e}^{-(k-k')^2(t-t')}\mathrm{e}^{-(k+l')^2(t-t')}W^\alpha_{k-k'+l}(t')\Big].\end{aligned} \tag{B.10}$$

The structure-factor (49) is obtained as,

$$\begin{aligned}W^\alpha_k(t) &= C_0^2(t-t',0)W^\alpha_k(t')+\frac{\varDelta}{(2\pi)^d}\Big[1-2C_0^2(t-t',0)\\ &+\frac{1}{\varGamma_0(t-t',0)}\frac{\varDelta}{(2\pi)^d}\int\mathrm{d}^dk'\\ &\times\int\mathrm{d}^dl'\mathrm{e}^{-(k-k')^2(t-t')}\mathrm{e}^{-(k+l')^2(t-t')}W^\alpha_{k-k'+l}(t')\Big].\end{aligned} \tag{B.11}$$

By taking inverse Fourier transform we obtain,

$$\begin{aligned}&\langle\phi^\alpha(x,t)\phi^\alpha(x',t)\rangle_\sigma-\langle\phi^\alpha(x,t)\rangle_\sigma\langle\phi^\alpha(x',t)\rangle_\sigma =\\ &\varDelta d^d(x-x')[1-2C_0^2(t-t',0)]+\frac{1}{\varGamma_0(t-t',0)}\left(\frac{\varDelta}{(2\pi)^d}\right)^2\\ &\times\int\mathrm{d}^dk\int\mathrm{d}^{d'}k\int\mathrm{d}^dl'\mathrm{e}^{-(k-k')^2(t-t')}\mathrm{e}^{-(k+l')^2(t-t')}\\ &\times W^\alpha_{k-k'+l'}(t')\end{aligned} \tag{B.12}$$

The above result implies that coarsening with respect an unrelated phase induces noise with a certain spatial correlation.

Appendix C: Response to uniform probing field

Here we study the linear response of the $O(n)$ Mattis model to an uniform external field. After describing the formal solutions, we obtained the response function in the one-step cycling of equilibrium states discussed in section 4.6.

C.1 Formal solution

In the $O(n)$ model in the spherical limit, response of the field at wavelength k is only due to perturbation at the same wavelength. A pulse staggered field $\hat h_k(t')$ at time t' induces a displacement of the projection field at time t as,

$$\delta\phi_k(t) = R_k(t,t')\delta\hat h_k(t'). \tag{C.1}$$

The response function [55] associated with wave-vector k reads,

$$R_k(t,t') = \frac{\mathrm{e}^{-k^2(t-t')}}{\varGamma(t,t')}, \tag{C.2}$$

where $\varGamma(t,t')$ is defined as (47).

Now let us consider the induced response $\delta\psi(x,t)$ due to a uniform pulse field $\delta h_{\mathrm{uni}}(t')$ applied at time $(t>)t'$. For simplicity, we assume that the system continues to coarsen with respect to the same equilibrium state between t' and t'. The relation (12) implies that the pulse of the uniform field $\delta h_{\mathrm{uni}}(t')$ induce the pulse of the staggered field at wavelength k as,

$$\delta\hat h_k(t') = \int\mathrm{d}^dy\mathrm{e}^{-\mathrm{i}ky}\sigma(y)\delta h_{\mathrm{uni}}(t'). \tag{C.3}$$

Then using the relation (38), the induced response of the real spin configuration becomes,

$$\begin{aligned}\delta\psi(x,t) &= \sigma(x)\delta\phi(x,t)\\ &= \sigma(x)\int\frac{\mathrm{d}^dk}{(2\pi)^d}\mathrm{e}^{\mathrm{i}kx}\delta\hat\phi_k(t)\\ &= \sigma(x)\int\frac{\mathrm{d}^dk}{(2\pi)^d}\mathrm{e}^{\mathrm{i}kx}R_k(t,t')\\ &\times\int\mathrm{d}^dy\mathrm{e}^{-\mathrm{i}ky}\sigma(y)\delta h_{\mathrm{uni}}(t').\end{aligned} \tag{C.4}$$

Finally the response function to uniform field is obtained using (40) and (59) as,

$$R_{\rm uni}(t,t') \equiv \frac{\langle \delta\psi(t)\rangle_\sigma}{\delta h_{\rm uni}(t')} = \frac{\Delta}{(2\pi)^d}\int {\rm d}^d k R_k(t,t') = \frac{R^{\rm eq}_{\rm uni}(\tau)}{\sqrt{\Gamma(t,t')}} \quad \text{(C.5)}$$

where

$$R^{\rm eq}_{\rm uni}(\tau) = \Gamma_0(\tau/2,0) \quad \text{(C.6)}$$

It is convenient to define re-scaled response,

$$\tilde{R}(t,t') \equiv \frac{R_{\rm uni}(t,t')}{R_{\rm eq}(t-t')} = \frac{1}{\sqrt{\Gamma(t,t')}}\cdot \quad \text{(C.7)}$$

In the case of relaxation starting from random initial condition we obtain the re-scaled response using (C.5), (C.6) and (59) as,

$$\tilde{R}_0(t,t') \equiv 1/\sqrt{\Gamma_0(t,t')} = \left(\frac{t}{t'}\right)^{-d/4}. \quad \text{(C.8)}$$

C.2 Response function after one-step cycling

Here we study the behavior of the response function after one-step cycling of the equilibrium states discussed in Section 4.6. The response function in the third stage of the one-step cycling $t_{\rm w3}+t_{\rm w2}+t_{\rm w1} > t(t') > t_{\rm w2}+t_{\rm w1}$ is obtained formally using (C.5, C.6) as,

$$\tilde{R}_{\rm III}(t,t')) = \frac{1}{\sqrt{\Gamma_{1-{\rm step}}(t,t')}} = \sqrt{\frac{\Gamma_{1-{\rm step}}(t',t_{\rm w2}+t_{\rm w1})}{\Gamma_{1-{\rm step}}(t,t_{\rm w2}+t_{\rm w1})}} \quad \text{'third stage'}. \quad \text{(C.9)}$$

Here the $\Gamma_{1-{\rm step}}$ factor is the one obtained in (96) which can be rewritten as,

$$\Gamma_{1-{\rm step}}(t,t_{\rm w2}+t_{\rm w1}) = [m^2_{\rm mem}(t-s,t_{\rm w2},t_{\rm w1}) + m^2_{\rm rej}(t-s,t_{\rm w2},t_{\rm w1}) + \tilde{m}^2(t-s,t_{\rm w2},t_{\rm w1})] \times \Gamma_{1-{\rm step}}(t,s)|_{s=t_{\rm w2}+t_{\rm w1}}. \quad \text{(C.10)}$$

(The same form holds for $\Gamma_{1-{\rm step}}(t',t_{\rm w2}+t_{\rm w1})$.) The three weights $m^2_{\rm mem}$, $m^2_{\rm rej}$ and $\tilde{m}^2$ describes 'memory' and 'rejuvenation' as we discussed in in Section 4.4.2. The sum of them equals 1 by definition.

In the inner-coarsening regime, we found that $m^2_{\rm rej} \sim 1$ while others are negligible. On the other hand, in the plateau and outer-coarsening regime, we found that $m^2_{\rm mem} \sim 1$ while others are negligible. Here we are assuming the case of wide separation a) $t_{\rm w1} \gg t_{\rm w2}$. In the inner- and outer-coarsening regime, th re-scaled response function becomes,

$$\tilde{R}_{\rm III}(t,t') \simeq \tilde{R}_0(t-t_{\rm w2}-t_{\rm w1}, t'-t_{\rm w2}-t_{\rm w1}) \quad \text{inner-coarsening regime} \quad \text{(C.11)}$$

$$\tilde{R}_{\rm III}(t,t') \simeq \tilde{R}_0(t-t_{\rm w2}, t'-t_{\rm w2}) \quad \text{plateau/outer-coarsening regime.} \quad \text{(C.12)}$$

References

1. A.J. Bray, M.A. Moore, Phys. Rev. Lett. **58**, 57 (1987).
2. D.S. Fisher, D.A. Huse, Phys. Rev. B **38**, 386 (1988).
3. D.S. Fisher, D.A. Huse, Phys. Rev. B **43**, 10728 (1991).
4. M. Nifle, H.J. Hilhorst, Phys. Rev. Lett **68**, 2992 (1992); M. Nifle, H.J. Hilhorst, Physica A **193**, 48 (1993).
5. D.S. Fisher, D.A. Huse, Phys. Rev. B **38**, 373 (1988).
6. G.J.M. Koper, H.J. Hilhorst, J. Phys. France **49**, 429 (1988).
7. E. Vincent, J. Hammann, M. Ocio, in *Recent Progress in Random Magnets* (World Scientific, Singapore, 1992).
8. E. Vincent, J. Hammann, M. Ocio, J.-P. Bouchaud, L.F. Cugliandolo, in *Proceeding of the Sitges Conference on Glassy Systems*, edited by E. Rubi (Springer, Berlin, 1996), `cond-mat/9607224`.
9. Ph. Refregier, E. Vincent, J. Hamman, M. Ocio, J. Phys. France **48**, 1533 (1987).
10. E. Vincent, J.P. Bouchaud, J. Hamman, F. Lefloch, Philos. Mag. B. **71**, 489 (1995).
11. F. Lefloch, J. Hammann, M. Ocio, E. Vincent, Europhys. Lett. **18**, 647 (1992).
12. P. Nordblad, P. Svedlindh, in *Spin Glasses and Random Fields*, *Series on Directions in Condensed Matter Physics* Vol. 12, edited by A.P. Young (World Scient., 1998), pp. 1–27 and references therein.
13. J.O. Andersson, J. Mattson, P. Nordblad, Phys. Rev. B **48**, 13977 (1993).
14. T. Jonsson, K. Jonason, O. Jonsson, P. Nordblad, Phys. Rev. B **59**, 8770 (1999).
15. K. Jonason, E. Vincent, J. Hamman, J.P. Bouchaud, P. Nordblad, Phys. Rev. Lett. **81**, 3243 (1998).
16. K. Jonason, P. Nordblad, E. Vincent, J. Hamman, J.P. Bouchaud, Eur. Phys. J. B **13**, 99 (2000).
17. L. Bellon, S. Ciliberto, C. Laroche, Europhys. Lett. **51**, 551 (2000), `cond-mat/9905160`.
18. H. Mamiya, I. Nakatani, T. Furubayashi, Phys. Rev. Lett. **82**, 4332 (1999); P. Jönsson, M.F. Hansen, P. Nordblad, Phys. Rev. B **61**, 1261 (2000).
19. E. Vincent, V. Dupuis, M. Alba, J. Hammann, J.-P. Bouchaud, Europhys. Lett. **50**, 674 (2000).
20. F. Alberici, P. Doussineau, A. Levelut, Europhys. Lett. **39**, 329 (1997); F. Alberici-Kious, J.P. Bouchaud, L.F. Cugliandolo, P. Doussineau, A. Levelut, Phys. Rev. Lett. **81**, 4987 (1998).

21. P. Doussineau, T. de Lacerda-Arôso, A. Levelut, Eur. Phys. J. B **16**, 455 (2000); J.-Ph. Bouchaud, P. Doussineau, T. de Lacerda-Arôso, A. Levelut, Eur. Phys. J. B (to be published).
22. R.L. Leheny, S.R. Nagel, Phys. Rev. B **57**, 5154 (1998).
23. J-P. Bouchaud, in *Soft and Fragile Matter*, edited by M.E. Cates, M.R. Evans (Institute of Physics Publishing, Bristol and Philadelphia, 2000), `cond-mat/9910387`.
24. J-P. Bouchaud, D.S. Dean, J. Phys. I France **5**, 265 (1995).
25. M. Mézard, G. Parisi, M.A. Virasoro, *Spin-Glass Theory and Beyond* (World Scientific, Singapore, 1988).
26. M. Sasaki, K. Nemoto, J. Phys. Soc. Jpn **69**, 2283 and 2642 (2000), and `cond-mat/0010443`.
27. L.F. Cugliandolo, J. Kurchan, Phys. Rev. Lett. **71**, (1993), Philos. Mag. B **71**, 501 (1995); J. Phys. A **27**, 5749 (1994).
28. S. Franz, M. Mézard, Europhys. Lett. **26**, 209 (1994); Physica A **210**, 48 (1994).
29. L.F. Cugliandolo, P. Le Doussal, Phys. Rev. E **53**, 1525 (1996), Cugliandolo, J. Kurchan, P. Le Doussal, Phys. Rev. Lett. **76**, 2390 (1996).
30. J-P. Bouchaud, L.F. Cugliandolo, J. Kurchan, M. Mézard, in *Spin-glasses and random fields*, edited by A.P. Young (World Scientific, Singapore, 1997) and references therein.
31. L.F. Cugliandolo, J. Kurchan, Phys. Rev. B **60**, 922 (1999).
32. S. Miyashita, Prog. Theor. Phys. **69**, 714 (1983); H. Kitatani, S Miyashita, M. Suzuki, J. Phys. Soc. Jpn **55**, 865 (1986).
33. S. Miyashita, E. Vincent (in preparation).
34. E. Vincent (private communication).
35. I. Kondor, A. Vegso. J. Phys. A **26**, L641 (1993).
36. S. Franz, M. Ney-Nifle, J. Phys. A **28**, 2499 (1995).
37. G. Parisi, T. Rizzo (unpublished).
38. S. Franz (private communication).
39. J. Houdayer, O.C. Martin, Phys. Rev. Lett. **81**, 2554 (1998); *ibid.* Europhys. Lett. **49**, 794 (2000); F. Krzakala, O.C. Martin, Phys. Rev. Lett. **85**, 3013 (2000).
40. E. Marinari, G. Parisi, `cond-mat/0002457`, Phys. Rev. B **62**, 11677 (2000) and `cond-mat/0007493`.
41. M. Palassini, A.P. Young, Phys. Rev. B **60**, R9919 (1999); Phys. Rev. Lett. **83**, 5126, (1999); Phys. Rev. Lett. **85**, 3017 (2000); Phys. Rev. Lett. **85**, 3333 (2000). G. Katzgraber, M. Palassini, A.P. Young, `cond-mat/0007113`.
42. N. Kawashima, J. Phys. Soc. Jpn **69**, 987 (2000), N. Kawashima, T. Aoki, `cond-mat/9911120`.
43. M.A. Moore, H. Bokil, B. Drossel, Phys. Rev. Lett. **81**, 4252 (1998); and B. Drossel, H. Bokil, M.A. Moore, A.J. Bray, Eur. Phys. J. B **13**, 369 (2000). See also E. Marinari, G. Parisi, J.J. Ruiz-Lorenzo, F. Zuliani, Phys. Rev. Lett. **82**, 5176 (1999); H. Bokil, A.J. Bray, B. Drossel, M.A. Moore, Phys. Rev. Lett. **82**, 5177 (1999).
44. A. Alain Middleton, Phys. Rev. Lett. **83**, 1672 (1999), `cond-mat/0007375`.
45. N. Hatano, J.E. Gubernatis, `cond-mat/0008115`.
46. H. Rieger, J. Phys. I France **4**, 883 (1994).
47. T. Komori, H. Yoshino, T. Takayama, J. Phys. Soc. Jpn **69**, Suppl. A 215 (2000).
48. M. Picco, F. Ricchi-Tersenghi, F. Ritori, *Chaotic, memory and cooling rate effects in spin-glasses: Is the Edwards-Anderson model a good spin glass?*, `cond-mat/0005541`.
49. H. Kawamura, Phys. Rev. Lett. **68**, 3785 (1992); Int. J. Mod. Phys. C **7**, 345 (1996); K. Hukusima, H. Kawamura, Phys. Rev. E **81**, R1008 (2000).
50. M. Lederman, R. Orbach, J.M. Hamman, M Ocio, E. Vincent, Phys. Rev. B **44**, 7403 (1991).
51. J-P. Bouchaud, H. Yoshino, E. Vincent, M. Hammann (in preparation).
52. For a recent review of domain growth dynamics see A.J. Bray, Adv. Phys. **43**, 357 (1994) and A.J. Bray, in *Soft and Fragile Matter*, edited by M.E. Cates, M.R. Evans (Institute of Physics Publishing, Bristol and Philadelphia, 2000).
53. J.A.N. Filippe, A.J. Bray, Sanjay Puri, Phys. Rev. E **52**, 6082 (1995).
54. L.F. Cugliandolo, D.S. Dean, J. Phys. A **28**, 4213 (1995); J. Phys. A **28**, L453 (1995).
55. L. Berthier, Eur. Phys. J. B **17**, 689 (2000).
56. D.C. Mattis, Phys. Lett. A **56**, 421 (1976).
57. D.A. Huse, C.L. Henley, Phys. Rev. Lett. **54**, 2708 (1985).
58. M. Mézard, G. Parisi, J. Phys. I France **1**, 809 (1991).
59. L. Balents, D.S. Fisher, Phys. Rev. B **48**, 5949 (1993).
60. L. Balents, J.P. Bouchaud, M. Mézard, J. Phys. I France **6**, 1007 (1996).
61. M. Mézard, J. Phys. France **51**, 1831 (1990).
62. T. Hwa, D.S. Fisher, Phys. Rev. B **49**, 3136 (1994).
63. H. Kinzelbach, H. Honer, J. Phys. I France **3**, 1329 and 1901 (1993).
64. H. Yoshino, J. Phys. A **29**, 1421 (1996).
65. A. Barrat, Phys. Rev. E **55**, 5651 (1997).
66. H. Yoshino, Phys. Rev. Lett. **81**, 1493 (1998).
67. H. Yoshino (in preparation).
68. In large time limits, solution with finite μ becomes the same as $\mu = \infty$ and satisfies the normalization condition.
69. H. Yoshino, K. Hukushima, H. Takayama (unpublished).
70. F. Ritort, Phys. Rev. B **50**, 6844 (1994) and references therein.
71. M. Ney-Nifle, Phys. Rev. B **57**, 492 (1997) and references therein.
72. A. Billoire, E. Marinari, J. Phys. A **33**, L265 (2000).
73. D.A Huse, L-F Ko, Phys. Rev. B **56**, 14597 (1997).
74. B. Derrida, Phys. Rev. B **24**, 2613 (1981); J. Phys. Lett. **46**, L401 (1985).
75. J.P. Bouchaud, J. Phys. I France **2**, 1705 (1992).
76. A.G. Schins, A.F.M. Arts, H.W. de Wijn, Phys. Rev. Lett. **70**, 2340 (1993).
77. Y.G. Joh, R. Orbach, G.G. Wood, Phys. Rev. Lett. **82**, 438 (1999).
78. L.W. Bernardi, H. Yoshino, K. Hukushima, H. Takayama, A. Tobo, A. Ito, Phys. Rev. Lett. **86**, 720 (2001).
79. H. Rieger, in *Annual Review of Computational Physics II*, edited by D. Stauffer (World Scientific, Singapore, 1995) and references therein.
80. T. Komori, H. Yoshino, H. Takayama, J. Phys. Soc. Jpn **68**, 3387 (1999) and **69**, 1192 (2000).
81. K. Hukushima, Phys. Rev. E **60**, 3606 (1999).
82. K. Hukushima, H. Yoshino, H. Takayama, Prog. Theor. Phys. **138**, 568 (2000) and in preparation.